UC San Diego
UC San Diego Previously Published Works

Title

Topoisomerase 1 inhibition suppresses inflammatory genes and protects from death by inflammation.

Permalink

https://escholarship.org/uc/item/05d7v7t0

Journal

Science (New York, N.Y.), 352(6289)

ISSN

0036-8075

Authors

Rialdi, Alex
Campisi, Laura
Zhao, Nan
et al.

Publication Date

2016-05-01

DOI

10.1126/science.aad7993

Peer reviewed

Topoisomerase 1 inhibition suppresses inflammatory genes and protects from death by inflammation

Alex Rialdi[#,1,2], **Laura Campisi**[#,1,2], **Nan Zhao**[1,2], **Arvin Cesar Lagda**[1,2], **Colette Pietzsch**[3], **Jessica Sook Yuin Ho**[4], **Luis Martinez-Gil**[1,5], **Romain Fenouil**[6], **Xiaoting Chen**[7], **Megan Edwards**[1], **Giorgi Metreveli**[1,2], **Stefan Jordan**[8], **Zuleyma Peralta**[6], **Cesar Munoz-Fontela**[9], **Nicole Bouvier**[1], **Miriam Merad**[8], **Jian Jin**[10], **Matthew Weirauch**[7], **Sven Heinz**[11,12], **Chris Benner**[12], **Harm van Bakel**[6], **Christopher Basler**[1], **Adolfo García-Sastre**[1,2], **Alexander Bukreyev**[3], and **Ivan Marazzi**[1,2,†]

[1]Department of Microbiology, Icahn School of Medicine at Mount Sinai, New York, NY 10029, USA

[2]Global Health and Emerging Pathogens Institute, Icahn School of Medicine at Mount Sinai, New York, NY 10029, USA

[3]Department of Pathology, Microbiology, and Immunology, University of Texas Medical Branch, Galveston, TX 77555, USA

[4]Laboratory of Methyltransferases in Development and Disease, Institute of Molecular and Cell Biology, Singapore

[5]Department of Biochemistry and Molecular Biology, Universitat de Valencia, Valencia, Spain

[6]Icahn Institute for Genomics and Multiscale Biology, Icahn School of Medicine at Mount Sinai, New York, NY 10029, USA

[7]Center for Autoimmune Genomics and Etiology (CAGE) and Divisions of Biomedical Informatics and Developmental Biology, Cincinnati Children's Hospital Medical Center, Cincinnati, OH 45229, USA

[8]Department of Oncological Sciences, Tisch Cancer Institute and Immunology Institute, Icahn School of Medicine at Mount Sinai, New York, NY 10029, USA

[9]Heinrich Pette Institute, Leibniz Institute for Experimental Virology, Hamburg, Germany

[10]Department of Structural and Chemical Biology, Department of Oncological Sciences, and Department of Pharmacology and Systems Therapeutics, Icahn School of Medicine at Mount Sinai, New York, NY 10029, USA

[11]Department of Cellular and Molecular Medicine, University of California, San Diego, 9500 Gilman Drive, La Jolla, CA 92093, USA

[12]Salk Institute for Biological Studies, 10010 North Torrey Pines Road, La Jolla, CA 92037, USA

[#] These authors contributed equally to this work.

[†]Corresponding author. ivan.marazzi@mssm.edu.

Abstract

The host innate immune response is the first line of defense against pathogens and is orchestrated by the concerted expression of genes induced by microbial stimuli. Deregulated expression of these genes is linked to the initiation and progression of diseases associated with exacerbated inflammation. We identified topoisomerase 1 (Top1) as a positive regulator of RNA polymerase II transcriptional activity at pathogen-induced genes. Depletion or chemical inhibition of Top1 suppresses the host response against influenza and Ebola viruses as well as bacterial products. Therapeutic pharmacological inhibition of Top1 protected mice from death in experimental models of lethal inflammation. Our results indicate that Top1 inhibition could be used as therapy against life-threatening infections characterized by an acutely exacerbated immune response.

The innate immune response is a key defense mechanism against infections. Activation of innate immune cells relies on the expression of a large family of pattern recognition receptors (PRRs), which detect distinct conserved microbial structures, called pathogen-associated molecular patterns (PAMPs) (1, 2). The immunological response that follows PRR downstream signaling is then governed by the combinatorial expression of PAMP response genes (3).

Although the function of many of the PAMP response genes and their antiviral or inflammatory activity remains elusive, their expression is essential for the host defense against pathogens (4). Failure in regulating the induction and post-induction repression of these antimicrobial genes can alter the balance between pro- and anti-inflammatory states, often leading to detrimental effects for the host (5–7). Indeed, hyperactivation of antimicrobial genes has been suggested to be responsible for the high mortality rates during highly pathogenic infections (8, 9). Another well-known example is the syndrome called "septic shock," where the uncontrolled expression of proinflammatory genes in response to bacterial PAMPs leads to severe collateral effects, such as local and systemic tissue injury, which can often be lethal to the host (10). In these contexts, pharmacological inhibition of factors that control the magnitude of the innate immune response could be useful for therapy.

Here, we show that the enzyme topoisomerase 1 (Top1) exerts an activating role on the transcriptional response against infection in cells and at the organismal level. This effect is achieved via Top1-assisted transcriptional activation of proinflammatory genes. We demonstrate that chemical inhibition, as well as reduced expression of Top1, limits the overexpression of inflammatory genes characteristic of infection with influenza and Ebola viruses and bacterial products. Notably, Top1 inhibition rescues mortality in mouse models of lethal inflammation caused by over-exposure to bacterial and viral PAMPs. Our results suggest that Top1 inhibitors offer therapeutic efficacy for the treatment of diseases characterized by exacerbated innate immune responses.

Topoisomerase 1 promotes PAMP-induced gene expression

Our goal was to identify novel regulatory mechanisms controlling the transcriptional response to pathogens by the innate immune system. We designed a reporter assay to

compare the potency of the transcriptional response to viral PAMPs and its dependence on a chromatin environment (fig. S1A). We used both the influenza A virus strain PR8 NS1 and Sendai virus because they are known to be strong inducers of PAMP-mediated gene expression (fig. S1C) (11). We then selected nine chemical inhibitors (fig. S1B) with already known or inferred chromatin targets and gauged their activity at various concentrations (fig. S1C) (12–20).

Our analysis revealed that flavopiridol (FVD), thienotriazolodiazepine [(+)-JQ1], and camptothecin (CPT) effectively inhibit the interferon-β (IFN-β)–driven transcription from chromatinized templates (Fig. 1A and fig. S1C). These observations were further reinforced by the efficacy of the three compounds in suppressing the endogenous expression of two key PAMP-induced genes—those encoding IFN-β and IFIT1 (IFN-induced protein with tetratricopeptide repeats 1)—in the human lung epithelial cell line A549 at 4 hours and 12 hours after PR8 NS1 virus infection (Fig. 1B). Notably, our analysis was performed using all of the compounds at concentrations that do not induce cytotoxicity in treated cells (fig. S1D).

The cellular targets of FVD, (+)-JQ1, and CPT are P-TEFb (the inhibitor of positive transcription elongation factor b), BET proteins (bromodomain and extra-terminal motif), and Top1, respectively (20–22). P-TEFb, BET proteins, and Top1 are ubiquitously expressed and are thought to control basal transcriptional levels of many genes. However, recent studies showed that P-TEFb and BET protein inhibitors have a specific effect on genes induced by innate immune stimuli (23) and during oncogenic transformation (24), highlighting their usage in what is often referred to as epigenetic therapy (25). For this reason, our observation that FVD and (+)-JQ1 suppress PAMP-induced genes, as well as the validation that such an effect is phenocopied by small interfering RNA (siRNA)–mediated depletion of their cellular targets (fig. S2), was not surprising. In contrast, the impact of CPT treatment on PAMP-induced genes, although previously observed (26–28), was less expected in light of recent genome-wide analyses demonstrating that Top1 inhibition suppresses the expression of the majority of long genes (>100 kb) while inducing a fraction of smaller genes (29, 30). The inhibitory effect at long genes is believed to be caused by Top1-mediated resolution of topological constraints occurring on long templates as a result of RNA polymerase II (RNAPII) activity (29, 31). The activating effect is instead thought to be dependent on gene-specific features such as topology, promoter sequence, or indirect effects (30–33). A concentration-dependent effect of the inhibitor CPT is also known, whereby high concentration and prolonged treatment lead to DNA damage (34).

To analyze the role of Top1 independently of its chemical inhibition, we examined the effect of transient Top1 depletion via siRNA. We infected control (siCtrl) and Top1-depleted (siTop1) A549 cells with influenza PR8 NS1 virus and assessed global differences in gene expression by microarray analysis (Fig. 1C, fig. S3, and table S1). Upon infection, Top1 depletion significantly decreased expression of 84 genes in infected cells relative to controls (siCtrl) (Fig. 1C). Remarkably, none of the down-regulated genes were long, but they were highly enriched for transcripts encoding inflammatory cytokines and interferon-stimulated genes (ISGs) (Fig. 1C, fig. S3, A and B, and table S2). The expression of housekeeping genes was unaffected independently of their level of expression (fig. S3C), indicating that

Top1 depletion does not suppress gene expression "tout court" but predominantly affects genes induced in response to infection. Notably, our gene knockdown experiments rule out the possibility that the suppression of PAMP-induced genes that we observed is the consequence of CPT-mediated stabilization of covalent complexes or induced cell damage, which are known to be caused by high dosage and prolonged chemical inhibition of Top1 (fig. S1D) (29). To strengthen this point, we performed a washout experiment in the presence and absence of Top1 inhibition. As shown in Fig. 1D, the effect of Top1 inhibition on inflammatory genes was fully reversible upon drug washout, indicating the absence of any permanent change or damage in treated cells.

We then performed a global proteomic analysis in influenza virus-infected A549 cells in the presence and absence of CPT treatment. Mass spectrometry analysis indicates that the protein levels of PAMP-induced genes were compromised upon Top1 inhibition (Fig. 1E), as indicated by the representative proteins DDX60L [DEAD (Asp-Glu-Ala-Asp) box polypeptide 60-like], IFIT3, OAS (2′,5′-oligoadenylate synthetase), and NFBKIE. The production of housekeeping proteins was unaffected independently of their expression level [Fig. 1E; low expressed, HPRT (hypoxanthine-guanine phosphoribosyltransferase); high expressed, ACTB (β-actin)]. Overall, these results indicate that Top1 is required to up-regulate antiviral gene expression after recognition of viral PAMPs.

Top1 controls RNAPII activity at PAMP-induced gene loci

To confirm the specificity of Top1 activity in our system, we first investigated whether the inhibition of PAMP-induced genes could be reproduced using a different Top1 inhibitor. We therefore used topotecan (TPT), an FDA-approved Top1 inhibitor. Our results indicate that both CPT and TPT suppress virus-induced genes (Fig. 2A) but not viral entry or replication (fig. S4). This was further supported by the observed PAMP-induced gene suppression in response to infection with Sendai virus and polyinosinic-polycytidylic acid [poly(I:C)] treatment (fig. S5). We reproduced the inhibitory effect of CPT and TPT on PAMP-induced gene expression using a different cell line, the murine macrophage RAW 264.7 (fig. S6A). Top1 inhibition did not suppress the response to other stimuli such as estrogen signaling and heat shock, as indicated by analysis of prototypical target genes (fig. S7, A and B, respectively).

Furthermore, chemical inhibition and loss-of-function experiments in A549 cells indicated that class II topoisomerase enzymes (Top2) do not fully phenocopy Top1 activity during PAMP-responsive gene induction (fig. S8); along with previous observations (29, 35, 36), this finding suggests that inhibition of topoisomerases can elicit both cell type–specific and gene-specific effects. Notably, and in line with what others have recently shown (29), neither TPT- nor CPT-treated cells displayed DNA damage at the concentration we used (fig. S9).

We then characterized the genomic distribution of RNAPII and Top1 during infection in the presence and absence of Top1 inhibition. Our results show reduced promoter levels of RNAPII and Top1 at PAMP-induced genes in infected A549 cells (Fig. 2B) and macrophages (fig. S6B) when Top1 is inhibited. Notably, RNAPII and Top1 levels at housekeeping genes were not reduced as a result of Top1 inhibition (Fig. 2B and fig. S6B),

consistent with their unaffected gene expression (Fig. 2A and fig. S6A). Reduced RNAPII targeting at PAMP-induced loci was confirmed by chromatin immunoprecipitation sequencing (ChIP-seq) (Fig. 2C) and by analysis of the RNAPII tracks at representative PAMP-induced genes and housekeeping genes (Fig. 2D).

To link cause (Top1 inhibition) and effect (RNAPII levels at promoters), we devised a strategy to map the genomic distribution of Top1 inhibitors via chem-ChIP, a method used to reveal the genomic localization of drugs (37). In brief, we first synthesized an analog of TPT (we did not succeed with CPT), which is amenable for coupling with a derivative of biotin. This compound was called TPT-alkyne (TPT-A; Fig. 2E). TPT-A synthesis and experimental strategy are shown in fig. S10, A and B; the validation that TPT-A is as effective as TPT is shown in fig. S10, C and D. We then performed chem-ChIP and analyzed the distribution of TPT-A on chromatin. At basal state, TPT-A was enriched at promoters and gene bodies of active genes such as ACTB and HPRT genes (Fig. 2F), as expected from results showing that Top1 travels with elongating RNAPII and that Top1 is distributed across the genome (31, 38).

During infection, TPT-A distribution peaks at promoters of inducible genes IFIT1 and IFIT2 (Fig. 2F) but not into gene bodies, which suggests that the presence of the inhibitor does not allow RNAPII and Top1 into productive transcriptional cycles. Indeed, TPT-A distribution is inversely correlated with RNAPII and Top1 density only at promoters of PAMP-induced genes (Fig. 2B). This indicates that TPT-A suppression of Top1 activity leads to a specific inhibition of RNAPII targeting at most PAMP-responsive loci (Fig. 2C). These results (i) corroborate the absence of an effect of Top1 inhibition at housekeepers, (ii) indicate that such genes can escape the transcriptional consequences of Top1 inhibition (likely via Top2; fig. S8D), and (iii) designate a RNAPII activator-like function for Top1 at PAMP-induced loci.

Top1 facilitates expression of genes that require nucleosome remodeling for activation

Previous work has characterized how classes of inducible genes respond temporally to induction of Toll-like receptor (TLR; a class of PRRs) according to genetic and epigenetic features (39–42). These studies provide a framework for addressing the specificity of Top1's effect during viral PAMP stimulation.

We first selected the Top1-affected genes whose expression was up-regulated by more than a factor of 2 upon infection (Fig. 3 and table S1). Similarly to (40), we then characterized this gene set according to dependence on IRF3 (interferon regulatory factor 3) and the SWI/SNF (switch/sucrose nonfermenter)–nucleosome remodeling complex for transcriptional activation. To do so, we performed RNA interference (RNAi)–mediated depletion of the two catalytic subunits of the SWI/SNF complex, SMARCA2 and SMARCA4, before and after infection with influenza virus or IFN treatment (Fig. 3A). This resulted in four distinct classes of Top1-affected genes (Fig. 3B).

We found that the vast majority (75%) of genes controlled by Top1 were dependent on SWI/SNF nucleosome remodeling. At basal state, these genes (relative to SWI/SNF-independent genes and housekeeping genes) were almost devoid of TATA-binding protein (TBP) and RNAPII, and displayed high levels of histone H3 at their promoters (Fig. 4A). These features indicate that nucleosome remodeling at these genes precedes recruitment of RNAPII and transcriptional initiation. Upon infection, Top1-affected genes are linked to transcriptional induction (as measured by histone H4 acetylation; fig. S11) and to broad expression levels, as measured by RNAPII recruitment (Fig. 4A) and expression data (Fig. 4A, inset). Inhibition of Top1 led to diminished RNAPII and TBP with a concomitant re-integration of H3 at promoters (Fig. 4A).

Genes that require remodeling for their activation are dependent on coactivators (42) and possess unique chromatin features at basal state, namely low levels of active histone marks, low levels of preloaded RNAPII, and low CpG island content (40). All these identifying features were recapitulated in Top1-affected genes by using genome-wide analyses and mathematical modeling of public data sets (Fig. 4, B to D, fig. S12, and table S3).

Top1 inhibition suppresses the response to bacterial stimuli and proinflammatory cytokines

To understand whether Top1 is required to activate the expression of proinflammatory genes induced by stimuli other than viruses, we characterized the effect of Top1 inhibition after exposure to bacterial PAMPs and exogenous cytokines. First, we treated both epithelial and macrophage cell lines with the bacterial PAMP lipopolysaccharide (LPS). Top1 inhibition suppressed the expression of antimicrobial genes, as indicated by the transcriptional analysis of representative proinflammatory cytokines (Fig. 5, A and B). Accordingly, Top1 inhibition resulted in reduced levels of Top1 and RNAPII at promoters of the affected genes (fig. S13, A and B).

The expression of antimicrobial genes upon PRR stimulation induces the secretion of proinflammatory signals, which trigger the maturation and activation of other innate immune cells expressing the corresponding receptors (43). To further extend our findings on cells activated via stimulation by inflammatory cytokines, we incubated both A549 and RAW cells with exogenous IFN-β and tumor necrosis factor–α (TNF-α). We then monitored gene expression changes, as well as promoter levels of RNAPII and Top1, in untreated and Top1-inhibited cells. As shown by the expression of multiple target genes (fig. S14, A and B) and respective chromatin occupancies (fig. S14, C and D), repression of Top1 activity inhibited IFN-β– and TNF-α–induced gene expression in both cell types analyzed, paralleling our results using viral and bacterial stimuli.

Top1 protects against lethal inflammation in vivo

Together, our data suggested that Top1 inhibition could be an effective way to suppress the exacerbated response to pathogenic stimuli, prompting us to characterize the role of Top1 inhibition in vivo. We first analyzed whether in vivo preventive inhibition of Top1 activity rescued animals from lethal endotoxic shock. This was indeed the case, where 90% of

animals pretreated with CPT were rescued (Fig. 5C). The protective effect of Top1 inhibition in vivo is caused not by cellular damage (Fig. 5, F to H) but by suppression of inflammatory cytokines (Fig. 5, D and E).

To test the potential of Top1 inhibition therapy in a model of bacterial disease, we infected mice with *Staphylococcus aureus*, which is one of the predominant pathogens causing nosocomial infections and sepsis in humans (44). Our results indicate that therapeutic treatment with CPT allowed 70% of the mice to survive the lethal challenge (Fig. 6A). Because the inflammatory response against influenza is believed to be responsible for the enhanced susceptibility to pneumonia after secondary infection with *S. aureus* in both mice and humans (45), we also tested whether CPT treatment could reverse the outcome of viral-bacterial co-infection. For this, mice inoculated with the influenza virus PR8 (H1N1 PR8 A/ Puerto Rico/8/1934 strain) were treated with CPT at 12, 24, and 36 hours after infection. Three days after viral infection, mice received a challenge with *S. aureus*. As shown in Fig. 6B, CPT treatment rescued 94% of the animals from the lethal co-infection challenge without impairing the differentiation of virus-specific CD8 T cells into IFN-γ– and TNF-α– producing effector cells (fig. S15). Strikingly, a similar protective effect (90% rescue of mortality) was also present when therapeutically inhibiting Top1 in an endotoxin-induced mouse model of acute liver failure, where the pathology is caused by high levels of secreted cytokines such as TNF-α (Fig. 6C) (46). These data suggest that in experimental models of lethal inflammation, therapeutic Top1 inhibition provides meaningful protection at the organismal level.

Finally, because an elevated mortality rate associated with an exacerbated proinflammatory response and clinical symptoms similar to septic shock is also observed in humans after infection with highly pathogenic viruses, we focused on *Zaire ebolavirus* (Ebola virus), which recently caused a large outbreak of illness with a high fatality rate in West Africa (47). We profiled the global gene expression response during Ebola (wild-type strain Zaire-Mayinga) infection in the human leukemic cell line THP-1 in the presence and absence of Top1 inhibition. Our analysis shows that Ebola virus–induced genes encoding interleukin-8 (IL-8), IL-1β, and TNF are suppressed by Top1 inhibition (Fig. 7 and table S4). Overall, these data highlight a protective role for Top1 inhibition during infections both in vitro and in vivo.

Discussion

Topoisomerase activities are required at all genes to resolve topological constraints that result from RNAPII activity. Recent work (29, 30) has shown that short and reversible Top1 inhibition specifically suppresses the expression of long genes. This indicated a differential susceptibility of genes to Top1 inhibition and redundant Top1 activities at the promoters of housekeepers. Our results provide evidence that during infection, short and reversible inhibition of Top1, as well as Top1 depletion, specifically suppresses genes induced by microbial agents. Our study reveals a gene-specific activator-like role for Top1. Concordantly, such an effect was shown using in vitro transcriptional assays (32, 33). The consequence of Top1 inhibition during infection is a suppression of RNAPII recruitment at PAMP-induced promoters. This effect is more prominent at genes with a bigger difference in

the levels of RNAPII at basal and induced states, which explains why compromising Top1 function affects inducibility of PAMP-responsive genes. The specificity of Top1 inhibition is then geared toward genes that are not prone to immediate activation but require coactivator (IRF3) assisted nucleosome remodeling. Other gene-specific co-transcriptional events such as the dynamics of pause release and elongation, along with RNA stability or transport, are likely to contribute to PAMP gene suppression by Top1 inhibition.

At the mechanistic level, Top1 inhibitors may create a local chromatin environment that is non-permissive to transcription, or alternatively, could titrate out new recruitment of Top1. Both scenarios would lead to defects in RNAPII recycling and reinitiation and would cause the observed suppressive effect at pathogen-induced genes. Because Top1 facilitates the expression of inflammatory genes, Top1 depletion or chemical inhibition during infection reduces the immune response associated with microbial recognition. This effect was evident in vitro by chemical inhibition of Top1 causing suppression of both virus-induced and inflammatory signal–induced host gene expression, and in vivo by displaying protective effects in mouse models of lethal inflammation. The cellular response against microbes is essential in protecting us against infection, but its hyperactivation can have fatal consequences. Our results suggest that a Top1 inhibition therapy could be useful in many instances, such as in pandemics and many congenital deficiencies, whereby an overt immune response is acutely induced.

Materials and methods

Cell lines and viruses

The following cell lines were originally obtained from the American Type Culture Collection (ATCC): A549 cells (adenocarcinomic human alveolar basal epithelial cells), 293T cells (human embryonic kidney cells), RAW 264.7 cells (mouse leukemic monocyte macrophage cell line), and HTBE cells (human primary bronchial/tracheal epithelial cells).

The 293T-FF cell line was generated by transfection with the plasmid pGL4.17-IFN-FF, encoding a cassette with the firefly luciferase gene under the control of the murine IFN-β promoter, as previously described (48), and was a gift from P. Palese.

Cells were maintained in culture at 37°C with 5% CO_2 in Dulbecco's minimal essential medium (DMEM, Gibco, Life Technologies) supplemented with 2 mM glutamine (Life Technologies), 10% fetal bovine serum (FBS; Hyclone), penicillin (100 U/ml; Life Technologies), and streptomycin (100 μg/ml; Gibco, Life Technologies).

The influenza virus PR8 NS1, which is the H1N1 PR8 A/Puerto Rico/8/1934 strain lacking the expression of the NS1 protein, was propagated in Madin-Darby canine kidney (MDCK) cells expressing the viral nonstructural protein 1 (NS1) (49). The influenza virus PR8 expressing green fluorescent protein (GFP) (PR8-GFP) and deficient for the viral protein hemagglutinin (HA) was propagated in MDCK-HA–expressing cells (50).

The influenza virus H3N2, which is the strain A/Philippines/2/82, was propagated in 10-day-old embryonated chicken eggs and was a gift from F. Kramer.

The Sendai virus (SeV), Cantell strain, was propagated in 10-day-old embryonated chicken eggs (51), and was a gift from P. Palese.

Viral infections using the strains described above were performed at a multiplicity of infection (MOI) of 3 and cells were analyzed at different time points as indicated in the figures.

Infections with the Ebola virus were performed in THP-1 cells, a human monocytic cell line that naturally expresses several PRRs. We used the wild-type Ebola Zaire-Mayinga strain and its VP-35 mutant, which fails to block the type I interferon response in the host (52). Cells were recovered 24 hours after Ebola infection.

IRF3 dependent genes were compiled from the literature and cross-compared with a list of genes induced by IRF3-5D in STAT1$^{-/-}$ cells (courtesy of S. Tripathi).

Cell viability assay

The Cell Titer Glo Cell Viability Assay (Promega) detects adenosine triphosphate (ATP) levels as a function of cell viability, and was used according to manufacturer's specifications. Briefly, cells were seeded into 96-well plates (5000 cells/well), and 18 hours later, 25 μl of fresh media containing the indicated compounds (serially diluted) were included. After 6 hours of incubation, 50 μl of CellTiterGlo was added and the luminescence was measured. Vehicle-treated cells were used to normalize (100%) the ATP activity.

The CytoTox 96 Non-Radioactive Cytotoxicity Assay (Promega), a colorimetric assay measuring the release of the cellular enzyme lactate dehydrogenase (LDH), was also used according to manufacturer's specifications.

Inhibitors and cell treatments

Cell culture—CPT (Sigma) was dissolved in a 4:1 mixture of chloroform and methanol at a concentration of 0.5 mM, heated at 55°C until fully dissolved and then added to cells in DMEM medium at a final concentration of 0.5 μM. TPT (Sigma) and TPT-A were dissolved in dimethyl sulfoxide (DMSO, Fisher) at the concentration of 100 μM and then added to cells in DMEM medium at a final concentration of 100 nM. FVD and (+/−)-JQ1 (both from Sigma) were dissolved in DMSO at a concentration of 0.5 mM and then added to cells in DMEM medium at a final concentration of 0.5 μM. Doxorubicin (Sigma) was dissolved in water at a concentration of 50 μM and then added to cells in DMEM medium at final concentrations of 0.5 and 5 μM.

All the compounds and the vehicle control DMSO were added to the cell cultures at 1 hour before and after stimulation or infection.

Lipopolysaccharide (LPS, Sigma, tlrl-3pelps) was added to cells in DMEM medium at a final concentration of 100 ng/ml for 2 hours. TNF-α (Sigma, human: T0157, mouse: T7539), IFN-β (PBL Assay Science, human: 11415-1, mouse: 12400-1), and poly(I:C) (Sigma, P1530) were added to cells in DMEM medium for 4 hours at final concentrations of 10 ng/ml, 100 U/ml, and 10 μg/ml, respectively.

For hormone treatment, A549 cells were grown in DMEM containing 5% charcoal-dextran–treated FBS (Sigma) for 2 days before addition of 17β-estradiol (10 nmol/liter; Sigma, E2758).

For heat shock, A549 cells were incubated at 42°C for 2 hours.

In vivo experiments—CPT was dissolved in a 4:1 mixture of chloroform and methanol, followed by heating at 55°C until fully dissolved. CPT was then brought up with water to the necessary volume corresponding to 200 μl per mouse and centrifuged for 5 min at 4000 rpm. The top aqueous fraction, containing the CPT, was recovered and dissolved at a final concentration of 30 mg/kg of mouse weight in 200 μl of water for each injection.

Immunofluorescence

A549 and RAW 264.7 cells were cultured on cover slips overnight and then treated with 0.5 and 10 μM CPT or 100 nM and 10 μM TPT 1 hour before and after infection with PR8 NS1 or H3N2 viruses. At 6 hours after infection, cells were fixed for 10 min at 4°C in 4% formaldehyde (EMS). Cover slips were washed in phosphate-buffered saline (PBS; Life Technologies) and cells were permeabilized for 10 min at room temperature in 0.5% NP-40 (Sigma). Cover slips were washed again in PBS and nonspecific binding was blocked by incubation for 30 min at room temperature with a solution containing 3% BSA (Sigma) in PBS. Cells were then probed for 2 hours with a rabbit anti-phospho-histone H2A.X antibody (Cell Signaling), followed by detection with Alexa Fluor 488-conjugated (green) goat anti-rabbit immunoglobulin G (IgG) (heavy and light chain, Life Technologies). DNA was counterstained with 4′,6-diamidino-2-phenylindole (DAPI, Thermo Scientific).

For visualization of the PR8-GFP virus, an EVOS FL (Thermo Scientific) microscope was used.

Quantitative polymerase chain reaction (qPCR)

For RNA extraction, cells were homogenized with QIAshredder columns; RNA was extracted using the RNeasy Mini Kit and then treated with the RNase-free DNase kit (all Qiagen). Proteins were also simultaneously recovered from cell lysates by acetone precipitation of the flow-through from RNeasy spin columns, according to manufacturer's instructions.

cDNA was in vitro transcribed using a High-Capacity cDNA RT Kit (Thermo Fisher Scientific) or a SuperScript III First-Strand Synthesis SuperMix (Life Technologies). qPCR was performed using the iTaq Universal SYBR Green One-Step Kit (Bio-Rad) according to manufacturer's instructions.

The statistical significance of all pairwise comparisons in qPCR assays' change in cycling threshold (ΔC_T) values was determined with a two-tailed Student's t test under the assumption of equal variances between groups. We did not find significant differences (false discovery rate, $q < 0.05$) between contrast groups in Levene's tests of equality of variances, or departures from normality as assessed by Shapiro-Wilk tests.

Primers

Primers were designed using the Primer3 online tool or by using already available primers from Harvard's PrimerBank database. Sequences of primers used for qPCR were as follows:

Human: β-actin forward, 5′-ACCTTCTACAATGAGCTGCG-3′; β-actin reverse, 5′-CCTGGATAGCAACGTACATGG-3′; GAPDH forward, 5′-GCAAATTCCATGGCACCGT-3′; GAPDH reverse, 5′-GCCCCACTTGATTTTGGAGG-3′; 18S forward, 5′-GTAACCCGTTGAACCCCATT-3′; 18S reverse, 5′-CCATCCAATCGGTAGTAGCG-3′; IFIT2 forward, 5′-AGGCTTTGCATGTCTTGG-3′; IFIT2 reverse, 5′GAGTCTTCATCTGCTTGTTGC-3′; IFIT1 forward, 5′-TTCGGAGAAAGGCATTAGA; IFIT1 reverse, 5′-TCCAGGGCTTCATTCATAT; IFNB1 forward, 5′-TCTGGCACAACAGGTAGTAGGC; IFNB1 reverse, 5′-GAGAAGCACAACAGGAGAGCAA; HPRT1 forward, 5′-GAAAAGGACCCCACGAAGTGT; HPRT1 reverse, 5′-AGTCAAGGGCATATCCTACAACA; BRD4 forward, 5′-GAGCTACCCACAGAAGAAACC; BRD4 reverse, 5′-GAGTCGATGCTTGAGTTGTGTT; IL-1β forward, 5′-ATGATGGCTTATTACAGTGGCAA; IL-1β reverse, 5′-GTCGGAGATTCGTAGCTGGA; IL-6 forward, 5′-ACTCACCTCTTCAGAACGAATTG; IL-6 reverse, 5′-CCATCTTTGGAAGGTTCAGGTTG; IL-8 forward, 5′-TTTTGCCAAGGAGTGCTAAAGA; IL-8 reverse, 5′-AACCCTCTGCACCCAGTTTTC; CDK9 forward, 5′-ATGGCAAAGCAGTACGACTCG; CDK9 reverse, 5′-GCAAGGCTGTAATGGGGAAC; CCNT1 forward, 5′-ACAACAAACGGTGGTATTTCACT; CCNT1 reverse, 5′-CCTGCTGGCGATAAGAAAGTT; CXCL10 forward, 5′-GTGGCATTCAAGGAGTACCTC-3′; CXCL10 reverse, 5′-TGATGGCCTTCGATTCTGGATT-3′; IFIT3 forward, 5′-AGAAAAGGTGACCTAGACAAAGC-3′; IFIT3 reverse, 5′-CCTTGTAGCAGCACCCAATCT-3′; ZFP36 forward, 5′-GAGAACAAATTCCGGGACCG-3′; ZFP36 reverse, 5′-GCGTGGAGTTGATCTGGGAG-3′; CCL5 forward, 5′-CCAGCAGTCGTCTTTGTCAC-3′; CCL5 reverse, 5′-CTCTGGGTTGGCACACACTT-3′; GBP1 forward, 5′-AACGACAGGGTCCAGTTGCTGAAAG; GBP1 reverse, 5′-TAGGGGTGACAGGAAGGCTCTGG; OASL forward, 5′-CTGATGCAGGAACTGTATAGCAC; OASL reverse, 5′-CACAGCGTCTAGCACCTCTT; IFIH1 forward, 5′-TCACAAGTTGATGGTCCTCAAGT; IFIH1 reverse, 5′-CTGATGAGTTATTCTCCATGCCC; IFI6 forward, 5′-GGTCTGCGATCCTGAATGGG; IFI6 reverse, 5′-

TCACTATCGAGATACTTGTGGGT; OAS2 forward,5′-
ACGTGACATCCTCGATAAAACTG; OAS2 reverse, 5′-
GAACCCATCAAGGGACTTCTG; SPRY2 forward, 5′-
CCTACTGTCGTCCCAAGACCT; SPRY2 reverse, 5′-
GGGGCTCGTGCAGAAGAAT; DDX58 forward, 5′-
TGCGAATCAGATCCCAGTGTA; DDX58 reverse, 5′-
TGCCTGTAACTCTATACCCATGT; RSAD2 forward, 5′-
TTGGACATTCTCGCTATCTCCT; RSAD2 reverse, 5′-
AGTGCTTTGATCTGTTCCGTC; TRIM22 forward, 5′-
AATGTGCTGGATAACCTGGCA; TRIM22 reverse, 5′-
TCTACTGACGATCCCCTCAAC; ISG15 forward, 5′-
CGCAGATCACCCAGAAGATCG; ISG15 reverse, 5′-
TTCGTCGCATTTGTCCACCA; UBE2L6 forward, 5′-
TGGACGAGAACGGACAGATTT; UBE2L6 reverse, 5′-
GGCTCCCTGATATTCGGTCTATT; TRIM21 forward, 5′ -
TCAGAGCTAGATCGAAGGTGC; TRIM21 reverse, 5′-
ACTCACTCCTTTCCAGGACAAT; IFITM1 forward, 5′-
GGGCCTTCTGGATTCCGAG; IFITM1 reverse, 5′-
CGTGGGGTTGGTCATCGTC; HERC5 forward, 5′-
GGTGAGCTTTTTGCCTGGG; HERC5 reverse, 5′-
TTCTCCGGCAGAAATCTGAGC; CDKN2C forward, 5′-
GGGGACCTAGAGCAACTTACT; CDKN2C reverse, 5′-
CAGCGCAGTCCTTCCAAAT; ISG20 forward, 5′-
TCTACGACACGTCCACTGACA; ISG20 reverse, 5′-
CTGTTCTGGATGCTCTTGTGC; ZC3HAV1 forward,5′-
TCACGAACTCTCTGGACTGAA-3′;ZC3HAV1 reverse, 5′-
ACTTTTGCATATCTCGGGCATAA-3′; JUN forward, 5′-
ATCAAGGCGGAGAGGAAGCG-3′; JUN reverse, 5′-
TGAGCATGTTGGCCGTGGAC-3′; BAMBI forward, 5′-
ATGCTCTCCCGTTTGCACTAC-3′; BAMBI reverse, 5′-
AGGATCTTATCGTTGCTGAGGT-3′; MX2 forward, 5′-
CAGAGGCAGCGGAATCGTAA-3′; MX2 reverse, 5′-
TGAAGCTCTAGCTCGGTGTTC-3′; IFI44 forward, 5′-
GGTGGGCACTAATACAACTGG; IFI44 reverse, 5′-
CACACAGAATAAACGGCAGGTA; TNF-α forward, 5′-
CCTCTCTCTAATCAGCCCTCTG; TNF-α reverse, 5′-
GAGGACCTGGGAGTAGATGAG; GFPforward, 5′-
AAGCTGACCCTGAAGTTCATCTGC; GFP reverse, 5′-
CTTGTAGTTGCCGTCGTCCTTGAA; PR8 HA forward, 5′-
AAAGAAAGCTCATGGCCCAACC; PR8 HA reverse, 5′-
TCCTTCTCCGTCAGCCATAGCA; PR8 PB1 forward, 5′-
TCATGAAGGGATTCAAGCCG; PR8 PB1 reverse, 5′-
GGAAGCTCCATGCTGAAATTG; HSP70 forward, 5′-
CATCGCCTATGGGCTGGAC; HSP70 reverse, 5′-
GGAGAGAACCGACACATCGAA; HSP27 forward, 5′-

ACGGTCAAGACCAAGGATGG; HSP27 reverse, 5′-AGCGTGTATTTCCGCGTGA; PGR1 forward, 5′-TCCACCCCGGTCGCTGTAGG; PGR1 reverse, 5′-TAGAGCGGGCGGCTGGAAGT; TFF1 forward, 5′-TTGGAGAAGGAAGCTGGATGG; TFF1 reverse, 5′-ACCACAATTCTGTCTTTCACGG; GREB1 forward, 5′-GTGGTAGCCGAGTGGACAAT; GREB1 reverse, 5′-ATTTGTTTCCAGCCCTCCTT; TOP1 forward, 5′-AAGGTCCAGTATTTGCCCCAC; TOP1 reverse, 5′-ATTCATGGTCGAGCATTTTTGC; TOP2A forward, 5′-ACCATTGCAGCCTGTAAATGA; TOP2A reverse, 5′-GGGCGGAGCAAAATATGTTCC; TOP2B forward, 5′-TTGGACAGCTTTTAACATCCAGT; TOP2B reverse, 5′-GCACCATAACCATTACGACCAC; SMARCA2 forward, 5′-AGGGGATTGTAGAAGACATCCA; SMARCA2 reverse, 5′-TTGGCTGTGTTGATCCATTGG; SMARCA4 forward, 5′-AATGCCAAGCAAGATGTCGAT; SMARCA4 reverse, 5′-GTTTGAGGACACCATTGACCATA.

Mouse: Actb forward, 5′-TTACGGATGTCAACGTCACAGTTC; *Actb* reverse, 5′-ACTATTGGCAACGAGCGGTTC; *Mip1a* forward, 5′-CGAGTACCAGTCCCTTTTCTGTTC; *Mip1a* reverse, 5′-AAGACTTGGTTGCAGAGTGTCATG; *Il-6* forward, 5′-TGAGATCTACTCGGCAAACCTAGTG; *Il-6* reverse, 5′-CTTCGTAGAGAACAACATAAGTCAGATACC; *Ifit1* forward, 5′-GCCTATCGCCAAGATTTAGATGA; *Ifit1* reverse, 5′-TTCTGGATTTAACCGGACAGC; *Ifit2* forward, 5′-AGAACCAAAACGAGAGAGAGTGAGG; *Ifit2* reverse, 5′-TCCAGACGGTAGTTCGCAATG; *Mip-2* forward, 5′-GTCCCTCAACGGAAGAACCAA; *Mip-2* reverse, 5′-ACTCTCAGACAGCGAGGCACAT; *Rantes* forward, 5′-TGCCCACGTCAAGGAGTATTTC; *Rantes* reverse, 5′-TCCTAGCTCATCTCCAAATAGTTGATG; *Il-1*β forward, 5′-GCAACTGTTCCTGAACTCAACT; *Il-1*β reverse, 5′-ATCTTTTGGGGTCCGTCAACT.

Sequences of primers used for ChIP followed by qPCR were as follows:

Human: ACTB 5′ forward, GAGGGGAGAGGGGGTAAAA; ACTB 5′ reverse, AGCCATAAAAGGCAACTTTCG; IFIT1 5′ forward, AGAGGAGCCTGGCTAAGCA; IFIT1 5′ reverse, GGTTGCTGTAAATTAGGCAGC; IFIT2 5′ forward, TGCACTGCAACCATGAGG; IFIT2 5′ reverse, TGACTCAACAGCACTACCGA; IL-6 5′ forward, CCCAATAAATATAGGACTGGAGATG; IL-6 5′ reverse, GAGTTCATAGCTGGGCTCCT; IL-8 5′ forward, TATAAAAAGCCACCGGAGCA; IL-8 5′ reverse,

GCCAGCTTGGAAGTCATGTT; CXCL10 5′ forward,
CAGCAGAGGAACCTCCAGTC; CXCL10 5′ reverse,
TGATGTTCCTTACCTTGAATGC; IFIT3 5′ forward,
CGGAACAGCAGAGACACAGA; IFIT3 5′ reverse,
GGGAAAAACCCCTCAAACAT; ZFP36 5′ forward,
ACTTCAGCGCTCCCACTCT; ZFP36 5′ reverse,
AGTTGGAGAAGGGAGGCAAG; CCL5 5′ forward,
CGAATTTCCGGAGGCTATTT; CCL5 5′ reverse,
CGTGCTGTCTTGATCCTCTG; GBP1 5′ forward,
ATGAGGAAATCCCAGCCCTA; GBP1 5′ reverse,
TCCTTAGTTCACGAGCACTGG. OASL 5′ forward,
AAATGCTCCTGCCTCAGAAA; OASL 5′ reverse,
GGGACAGAGATGGCACTGAT; IFIH1 5′ forward,
GAAGGAGGTTCAGCAGTTGG; IFIH1 5′ reverse,
AGCACCTTGGAGAAGGGAGT; IFI6 5′ forward,
TGATGCCCACACTTCATAGC; IFI6 5′ reverse,
GGGAGGATCCACAAGTGATG; OAS2 5′ forward,
TTTCAGTTTCCTGGCTCTGG; OAS2 5′ reverse,
TGGATAAACCAACCCAGCTT; SPRY2 5′ forward,
AAAGAGAATTCGGAGCCAGA; SPRY2 5′ reverse,
ATCTGCCAGGAAAAGGGACT; DDX58 5′ forward,
CCTTTCACCTCTTTCCCAGA; DDX58 5′ reverse,
CTTTTCCAGACCGAATAGCTT; RSAD2 5′ forward,
CCAATGACAGGTTGCTCAGA; RSAD2 5′ reverse,
CAGCTGCTGCTTTCTCCTCT; TRIM22 5′ forward,
CTGAGTGCCTTGCCAGTACA; TRIM22 5′ reverse,
CAAATGAGTTTCCCCACAGG; ISG15 5′ forward,
GCTGAGAGGCAGCGAACTC; ISG15 5′ reverse,
CCCCACCTGTGACATCTGC; UBE2L6 5′ forward,
CCGGGACTCACGGTCTTT; UBE2L6 5′ reverse,
CGGAGCGAAGACTGGAAC; TRIM21 5′ forward,
GCTCAAGGATGGAGACTGGA; TRIM21 5′ reverse,
CCTCCCCTTTCCTCTCAGAC; IFITM1 5′ forward,
AACTGAAACGACAGGGGAAA; IFITM1 5′ reverse,
ACAGCCACCTCATGTTCCTC; HERC5 5′ forward,
ACCAGGCGTTCTCTCCTCTC; HERC5 5′ reverse,
CTGGGAAAGAGCCAGAGC; IFNB1 5′ forward,
GGAATCCAAGCAAGTTGTAGC; IFNB1 5′ reverse,
AACCTTTCGAAGCCTTTGCT; CDKN2C 5′ forward,
GCCGAGCCTCCTTAAAACTC; CDKN2C 5′ reverse,
ACAATTGCTGCTTCTGTTGC; ISG20 5′ forward,
GGTAGCCCAGGAGATGGAG; ISG20 5′ reverse,
CTCACGTCTGCCTCTCTGCT; ZC3HAV1 5′ forward,
CGCATCTGCATTTAGACGAA; ZC3HAV1 5′ reverse,
CTCAACAGGGCTCTCAGGAC; JUN 5′ forward,

CCGTTGCTGGACTGGATTAT; JUN 5′ reverse, CCCCAAGATCCTGAAACAGA; BAMBI 5′ forward, CGTGCTGTGGAGACCCTACT; BAMBI 5′ reverse, CCAGGAGCCCAGAAAAGTT; MX2 5′ forward, CCACAGCTCTCCCAGGATT; MX2 5′ reverse, TGTGGCATATGAACCACTCC; IFI44 5′ forward, TGAGAGAAGTTGGCATGCTG; IFI44 5′ reverse, AGCTGAGGGTAGCTGCTCTGT; IRF1 5′ forward, AAGAGGGAAGAAGGCAGAGG; IRF1 5′ reverse, CTTAGTCGAGGCAAGACGTG; KLF4 5′ forward, TCTCTCTGGTCGGGAAACTG; KLF4 5′ reverse, GCGCCGAGTTTGTTGATTTA; GAPDH 5′ forward, ACAGTCAGCCGCATCTTCTT; GAPDH 5′ reverse, TTCTCTCCGCCCGTCTTC.

Mouse: *Actb* 5′ forward, GGGCTACAGTGGGTGAAAGG; *Actb* 5′ reverse, GGGCTACAGTGGGTGAAAGG; *Ifit1* 5′ forward, TGAAAAGAGCACACCCCCTA; *Ifit1* 5′ reverse, CTCCTCAGAAACCTGCCTTG; *Ifit2* 5′ forward, AGCCACACCCGACTAACG; *Ifit2* 5′ reverse, CTTGGTGCTTTGAGGGATCT; *Il-6* 5′ forward, AATGTGGGATTTTCCCATGA; *Il-6* 5′ reverse, GCGGTTTCTGGAATTGACTATC; *Mip2-a* 5′ forward, GGGCTTTTCCAGACATCGT; *Mip2-a* 5′ reverse, TGAAGTGTGGCTGGAGTCTG.

Sequences of primers used for chem-ChIP followed by qPCR were as follows:

Human: ACTB upstream forward, CTGCAGAAGGAGCTCTTGGA; ACTB upstream reverse, GACCCACCCAGCACATTTAG; ACTB-1 forward, GAGGGGAGAGGGGGTAAAA; ACTB-1 reverse, AGCCATAAAAGGCAACTTTCG; ACTB-2 forward, GTCATCTTCTCGCGGTTGG; ACTB-2 reverse, GGCATCCTCACCCTGAAGTA; ACTB-3 forward, CCTACACCCACAACACTGTCT; ACTB-3 reverse, TGACCTGAGTCTCCTTTGGAA; ACTB-4 reverse, CAGGTCCAGACGCAGGAT; ACTB-4 reverse, GCCATGTACGTTGCTATCCA; ACTB-5 forward, GTGCCAGGGCAGTGATCT; ACTB-5 reverse, CTGTGGCATCCACGAAACTA; ACTB-6 forward, CTAAGTCATAGTCCGCCTAGAAGC; ACTB-6 reverse CTGTCCACCTTCCAGCAGAT; ACTB downstream forward, CGCCCAGTCTCCAGTCAC; ACTB downstream reverse, GTTGGGGTAGGGGGTCCA; HPRT1 upstream forward, TAGTCGGGGTTCTCCACAAA; HPRT1 upstream reverse, CCTTCAGATTTTGGACTCAACA; HPRT1-1 forward, GAAAATTCCCACGGCTACCT; HPRT1-1 reverse,

GGGAAAGCCGAGAGGTTC; HPRT1-2 forward,
GACAGAGTCTTGCTCTGTTTCC; HPRT1-2 reverse,
AAAATTAGCCGGGTGTGGT; HPRT1-3 forward,
GCCTGGGCTAGACTTTTGAG; HPRT1-3 reverse,
TGACAGGTGTCTGGTTCTGG; HPRT1-4 forward,
CTGGACCTCCTGGAATTGAG; HPRT1-4 reverse,
AAACACAGGTAGAACTATAAAAGCAAA; HPRT1-5 forward,
GATGCTCACCTCTCCCACAC; HPRT1-5 reverse,
CCCTGACTACCCATGTGTCC; HPRT1-6 forward,
TGTCATTAGTGAAACTGGAAAAGC; HPRT1-6 reverse,
CATGCAAAAAGCTCTACTAAGCA; HPRT1 downstream forward,
CGTCTGGGGTCATACAGGTT; HPRT1 downstream reverse,
CTGAGGGCAGGGATAGTTTG; IFIT1 upstream forward,
CAAGACTGCTGCCAAATTCA; IFIT1 upstream reverse,
CATGATCAGGCCATAAGCAA; IFIT1-1 forward,
AGAGGAGCCTGGCTAAGCA; IFIT1-1 reverse,
GGTTGCTGTAAATTAGGCAGC; IFIT1-2 forward,
AACAGGTTTTCGCAATCAGG; IFIT1-2 reverse,
CTTCCCAAGCAGATGTGGAT; IFIT1-3 forward,
AACATTTTTCTCGCTATGTGGA; IFIT1-3 reverse,
GACAGAAAGCAGATTAACAGTTGC; IFIT1-4 forward,
TTTTCATGGCTGTCATCAGATT; IFIT1-4 reverse,
TTCCACTCAGATTGGCAAGA; IFIT1-5 forward,
ACTATTTGAGATCCCTTGACATTT; IFIT1-5 reverse,
GATGTCAATACTACCCAAAGTGATCT; IFIT1-6 forward,
GAAATATGAATGAAGCCCTGGA; IFIT1-6 reverse,
GGCTGATATCTGGGTGCCTA; IFIT1 downstream forward,
AGCTGCAGCCTGAGAGTTTG; IFIT1 downstream reverse,
CCAGTCCCCATGATCTGAGT; IFIT2 upstream forward,
GAGGACTTTAAATGATACCAACACA; IFIT2 upstream reverse,
TTTCCCCCTTTTTATTGATGT; IFIT2-1 forward,
TGCACTGCAACCATGAGG; IFIT2-1 5′ reverse,
TGACTCAACAGCACTACCGA; IFIT2-2 forward,
TCAGAGAAAGAAGGCAGCAGA; IFIT2-2 reverse,
AAGACAGGGTCAGTGCACAA; IFIT2-3 forward,
AACCCAAAATCAAGCAGTGAA; IFIT2-3 reverse,
TGTGCATTTGCAGGATAGAGA; IFIT2-4 forward,
TCCCAATCAAAATGGGAGTG; IFIT2-4 reverse,
TGTGGCAGGATCACTTATGAA; IFIT2-5 forward,
CCAATCTGATAAAAGCTCAGAAA; IFIT2-5 reverse,
AGTTCTCCTTCATTTGCCTTT; IFIT2-6 forward,
GCAGCCCTGGAATGCTTAC; IFIT2-6 reverse,
CAGGCATAGTTTCCCCAGGT; IFIT2 downstream forward,
TGAGTCATAGTTTGTGTTATTTCTGA; IFIT2 downstream reverse,
GGATTCTGGAAAGGTAAAGAAAGA.

Transfection with siRNA

Transfection experiments were performed using the Lipofectamine RNAiMAX transfection reagents according to the manufacturer's instructions (Invitrogen). Cells were transfected with siRNA pools (all from Dharmacon) targeting the genes encoding human Top1, BRD4, CDK9, CCNT1, SMARCA2, SMARCA4, TOP2A, TOP2B, or with a control nontargeting pool, at a final concentration of 50 nM. Cells were used 48 hours after transfection, and the efficiency of gene knockdown was determined by qPCR or immunoblotting.

Microarray analysis

A549 cells were transfected with siRNA targeting the gene encoding Top1 or control nontargeting siRNA (siCtrl), then infected in triplicate with the PR8 NS1 virus (MOI = 3). Nontransfected cells were also infected, as a further control. RNA was isolated from infected and uninfected cells with a Qiagen RNeasy kit and 200 ng of RNA per sample was then used to prepare labeled RNA that was hybridized to Human HT-12 v4 Expression BeadChips (Illumina). Data were analyzed using the Genespring software (version 12.5).

To determine the effect of Top1 depletion on the magnitude of cell response during infection, raw signal values obtained from uninfected and infected cells in all siRNA treatments were quantile-normalized before being baseline-transformed to the medians of signal values for the corresponding uninfected siRNA-treated samples. For identification of probe sets with statistically significant differences in magnitude of response ($P < 0.01$), we conducted an analysis of variance (ANOVA) followed by a post hoc [Tukey's honest significant difference (HSD)] test.

We selected genes differentially expressed after treatment with siTop1 using a threshold of a factor of 1.5 change ($P < 0.01$) in their expression relative to siCtrl-treated cells. When indicated, infection-induced genes were identified as the ones showing a factor of 1.5 change ($P < 0.01$) in their expression in infected siCtrl-treated cells relative to uninfected siCtrl-treated cells.

All computations of P values were subjected to multiple-testing correction using the Benjamini-Hochberg method. For purposes of presentation, genes represented by multiple probe sets in the microarray were plotted in the heat maps as the averaged values of those probe sets.

To determine the effect of Top1 depletion under basal conditions, we normalized raw signal values from uninfected siRNA-treated cells by quantile before baseline-transforming them to the median of all samples. A statistical ANOVA test followed by a post hoc test was then conducted. Genes regulated by the siRNA targeting the Top1 gene were defined as genes with a factor of 1.5 change ($P < 0.01$) in their expression relative to the siCtrl controls. Normalized signal intensity values of a list of canonical housekeeping genes were also used to determine the overall effect of the depletion of Top1 in cells. A full list of the affected genes is shown in table S1.

We used Ingenuity Pathways Analysis software (Ingenuity Systems) for the identification of canonical pathways that showed "enrichment" among groups of genes with significant

changes in their expression by microarray analysis. The DAVID gene ontology analysis helped to identify genes associated with cytokine activity (53, 54). A right-tailed Fisher's exact test was used for calculation of *P* values determining the probability that each pathway assigned to a specific data set was due to chance alone.

Mice and related experiments

C57BL/6J female mice were purchased from The Jackson Laboratories and housed under specific pathogen-free conditions in the animal care facility at the Icahn School of Medicine at Mount Sinai (ISMMS). Mice were studied at 7 to 12 weeks of age. All experiments were approved by the institutional animal care and use committee and carried out in accordance with the *Guide for the Care and Use of Laboratory Animals* (NIH publication 86-23, revised 1985).

For the septic shock model, mice were injected intraperitoneally (i.p.) with 10 mg/kg of ultrapure LPS (from *E. coli* 0111:B4 strain-TLR4 ligand, InvivoGen) resuspended in 200 µl of water. For the preventive protocol, one group of mice received, after isoflurane anesthesia, a first retro-orbital intravenous injection with a dose of 30 mg/kg of CPT 30 min before LPS treatment followed by an i.p. challenge with the same dose of CPT 1 hour after LPS injection.

For the acute liver failure model, mice were injected i.p. with a mixture of 5 mg of D-(+)-galactosamine (Sigma) and 500 ng of ultrapure LPS (Invivogen) (referred to as D-GalN/LPS), in 200 µl of water. One group of mice was also injected i.p. with CPT (110 mg/kg) 1 hour before (preventive protocol) or 2 hours and 30 min after (therapeutic protocol) GalN/LPS treatment.

For the sepsis model using *Staphylococcus aureus* infection (subsp. *aureus* Rosenbach, FDA 209P strain, ATCC) bacteria were grown in Bacto Tryptic Soy Broth (BDbioscience) until stationary phase, washed, and suspended in PBS at 25×10^8 bacteria/ml and mice intravenously injected with 200 µl of the bacterial suspension. We then started the treatment 3 hours after infection, when animals presented the first clinical signs of disease (ruffled fur, diminished activity, and hunched posture). One group of mice received a first dose of 30 mg/kg of CPT intravenously, followed by IP injections of 45 mg/kg of CPT 24 and 48 hours later.

For the co-infection model, the influenza virus PR8 (H1N1 PR8 A/Puerto Rico/8/1934) was administered intranasally in sterile PBS in a volume of 50 µl at a titer of $0.3 \times LD_{50}$. Three days after influenza infection, *S. aureus* stocks were grown until exponential phase and resuspended in sterile PBS in a volume of 50 µl containing 5×10^8 bacteria per mouse for intranasal administration. Mice were anesthetized with ketamine-xylazine before all intranasal injections. One group of mouse received 75 mg/kg of CPT i.p. at 12, 24, and 36 hours after viral infections.

Survival significance in the in vivo experiments was calculated using a log-rank Mantel-Cox test with the Graphpad software Prism.

During all treatments, mice were daily weighed and monitored two to six times per day until the end of the experiment. We considered a loss >20% of the initial weight as a humane end point, according to the policy of the institutional animal care and use committee at ISMMS. In case of survival, animals were under observation twice per day for the following month and every week for additional months. We did not detect any side effect of the CPT treatment in mice monitored for at least 3 months.

Quantitative PCR in tissue samples—Spleens and lungs were homogenized in 1 ml of TRIzol Reagent (Life Technologies) using a mechanical homogenizer. RNA separation and isolation were performed using chloroform and isopropanol (both from Sigma), respectively, according to manufacturer's instructions (Life Technologies). cDNA synthesis and qPCR were performed as described above.

Cytokine detection—Quantitative mRNA analysis for inflammatory gene expression was conducted after RNA isolation from the spleens of untreated and CPT-treated mice 90 min after LPS injection.

To determine the cytokine concentration during the treatment, 50 μl of blood was collected retro-orbitally 4 hours after LPS injection. Serum and plasma were separated after centrifugation at 10,000 rpm for 10 min. Quantitative determination of GM-CSF, IL-1β, IL-6, and TNF-α in mouse serum was performed using a Mouse Inflammatory Magnetic 4-Plex Panel (Novex Life Technology), according to the manufacturer's instructions. Data was acquired using a Luminex 100/200 plate reader.

Cell suspensions and ex vivo restimulation—Cell suspensions were obtained after cutting the organs into small pieces followed by 30 min incubation at 37°C in DMEM containing collagenase D (1 mg/ml; Roche) and DNase (20 μg/ml; Roche). Tissue suspensions were then filtered through a 70-μm cell strainer (BD Falcon), and red blood cells were lysed using 1 ml of RBC Lysis Buffer (Affymetrix eBioscience).

For surface staining, cells were suspended in PBS containing 2% FBS, anti-mouse CD16/32 (Biolegend) and 0.1% NaN_3. For intracellular staining, cells were fixed in Fixation/Permeabilization buffer (eBioscience) and stained in Perm/Wash buffer (eBioscience).

For antigen-specific restimulation, cells were resuspended in complete [i.e., supplemented with 10% FBS, penicillin (100 μg/ml), streptomycin (100 μg/ml), and 1 nM sodium pyruvate] DMEM (Sigma) and restimulated with 100 nM peptide ASNENMETM derived from viral A/PR8/34 nucleo-protein (NP, 366 to 374 amino acids) (MBL) in the presence of Brefeldin A (Biolegend), and incubated for 6 hours at 37°C.

All antibodies were purchased from Biolegend: anti-mouse CD45 (clone 30-F11), CD11c (N418), CD11b (M1/70), Ly6C (HK 4.1), CD69 (H1.2F3), MHC-II (M5/114.15.2), CD8β (Ly-3), CD44 (IM7), CD3ε (17A2), CD45 (30-F11), TNF-α (MΠ6-XT22), IFN-γ (XMG1.2). Dead cells were discriminated using the Zombie Aqua Fixable Viability Kit (Biolegend), referred to as Life/Death dye.

Acquisition of stained cells was made with a BD LSRII flow cytometer (BD Bioscience); data were analyzed with FlowJo software (Treestar).

Antibodies and immunoblotting

Antibodies used were as follows: anti–β-actin (3700; Cell Signaling); anti-TOP2A (ab52934; Abcam), anti-TOP2B (ab58442; Abcam), anti-TOP1 (A302-589A; Bethyl), anti-FLAG-HRP (A8592; Sigma). Gradient gels were used according to the molecular weight of the proteins to be evaluated, followed by wet transfer on polyvinylidene fluoride membranes.

ChIP

The following antibodies were used: anti-RNAPII (clone 8WG16; Covance/BioLegend), anti–topoisomerase I (TOP1) (rabbit polyclonal anti-human IgG; Bethyl Laboratories; rabbit polyclonal anti-human/mouse serum; Abcam), anti–histone H3 (rabbit polyclonal IgG; Abcam), anti–TATA binding protein (rabbit polyclonal antiserum; Abcam), and anti–histone H4ac (rabbit polyclonal anti-human/mouse serum; Active Motif).

ChIP experiments were conducted as described (55). For experiments with ChIP followed by qPCR, cross-linking was performed for 10 min. For sonication, we used a refrigerated Bioruptor (Diagenode), which we optimized to generate DNA fragments of approximately 200 to 1000 base pairs (bp). Lysates were precleared for 3 hours using the appropriate isotype-matched control antibody (rabbit IgG; Cell Signaling) or anti-mouse IgG (Cell Signaling). The specific antibodies were coupled with magnetic paramagnetic beads (Dynabeads M-280 sheep anti-mouse IgG; Thermo-Fisher Scientific) bound to anti-mouse IgG or anti-rabbit IgG for 6 hours. Antibody-bound beads and chromatin were then immune-precipitated overnight at 4°C with rotation. After washing, reverse crosslinking was carried out overnight at 65°C. After digestion with RNase and proteinase K (Roche), DNA was isolated with a MinElute kit (Qiagen) and used for downstream applications. The statistical significance of ChIP qPCR analysis was determined with a two-tailed Student's paired *t* test.

ChIP-seq sample preparation and sequencing

After sonication (Bioruptor Pico, Diagenode), input and IP samples were analyzed on an Agilent Bioanalyzer (DNA High Sensitivity kit) to confirm that the fragment distributions were within the expected size range. Sheared Input and ChIP DNA samples were then end-repaired using NEBNext End Repair Module (New England BioLabs) and cleaned up using 1.5× AMPure XP beads (Beckman Coulter) according to the manufacturer's instructions, except for the final elution step, which we omitted. Next, A-tailing was done on beads using the NEBNext dA-Tailing Module (New England BioLabs), followed by addition of 20% polyethylene glycol (PEG)/NaCl in a 1.5× ratio to AMPure XP bead cleanup, again omitting the final elution step. Adaptor ligation was performed using the NEBNext Quick Ligation Module (New England BioLabs) and 80 µM DNA Multiplex Adaptor. Then, 20% PEG/NaCl was added in a 1.5× ratio followed by the AMPure XP cleanup. Samples were then eluted from beads and split into two aliquots. Each aliquot was amplified for 28 cycles using KAPA HiFi HotStart ReadyMix PCR Kit (Kapa Biosystems), 25 µM PE forward primer, and 25 µM indexed reverse primer. PCR reactions were cleaned using 1.5× of the AMPure XP beads

according to the manufacturer's protocol and selected on the basis of fragments with a size of 250 to 500 nucleotides on the BluePippin platform using 2% M1 Marker gels. Size selected libraries were cleaned using 1.8× of the AMPure XP beads and sequenced on the HiSEq 2500 platform in a 100-nucleotide single-end read format.

Adapters used for ligation—Adapter1, 5′ PGATCGGAAGAGCACACGTCT; Adapter2, 5′ ACACTCTTTCCCTACACGACGCTCTTCCGATC*T (* = phosphorothioate).

Barcode PCR primers—
5′AATGATACGGCGACCACCGAGATCTACACTCTTTCCCTACACGACGCTCTTCCG ATC*T,
5′CAAGCAGAAGACGGCATACGAGAT[NNNNNN]GTGACTGGAGTTCAGACGTGTG CTCTTCCGATC*T (where N corresponds to the barcode sequences used).

ChIP-seq data processing

ChIP-seq reads were trimmed for adapter sequences using "cutadapt." Reads were then filtered using "sickle" with a minimum quality threshold of 20 and retaining only sequences containing at least 20 bases. QC-filtered reads were then aligned against the human reference genome (GRCh37) using STAR, selecting only nonambiguous alignments and allowing up to five mismatches for each alignment. The resulting BAM files were processed using the R package "Pasha" with default parameters in order to exclude artifactual enrichments, estimate fragments elongation, and prepare genome-wide read coverage tracks in variable-step WIG format. WIG scores were finally rescaled for each sample by dividing all values by the average genome wide enrichment value.

Average profile computation—The average read coverage for selected genes was calculated across the annotated gene regions, including 2-kb flanking regions. For each gene, coverage in flanking regions was sampled across 167 equally spaced bins, and the resulting values were averaged across the upstream and downstream regions of all selected genes. Coverage across the annotated region of each gene was calculated in 666 equally spaced bins within the annotated start and end coordinates, and the resulting vectors were averaged across all genes and combined with the gene-flanking regions to create a composite average profile of 1000 points, covering selected annotations and 2 kb of each flanking region. All average profiles were normalized based on the average ChIP signal across the third quartile (i.e., last 50 to 75%) of the gene body of active genes [previously identified by Gro-seq profiling (56)], to account for differences in ChIP efficiency between experiments.

Chemical synthesis of TPT-A

An alkyne group was introduced to the 10-hydroxyl group of TPT through a Mitsunobu reaction (57), as the 10-hydroxyl of TPT does not contribute to the binding between human topoisomerase I covalently joined to double-stranded DNA and TPT [according to the reported x-ray crystal structure (58)]. TPT hydrochloride was dissolved in distilled water and further neutralized by adding (dropwise) a saturated solution of sodium bicarbonate ($NaHCO_3$) until the pH reached 9 to 10. Hydrochloride-free TPT was extracted from this

solution by washing the aqueous phase with dichloromethane (DCM) three times, combining the organic phase, drying it by incubation with sodium sulfate (Na_2SO_4) for 1 hour, and finally evaporating DCM under reduced pressure. The TPT was then fully dissolved together with 5 equiv of triphenylphospine (Ph_3P) and 5 equiv of propargyl alcohol in a small volume of anhydrous tetrahydrofuran (THF). Five equiv of diethyl azodicarboxylate (DEAD) was then added dropwise into the solution. The reaction was monitored using thin-layer chromatography (TLC). The reaction time was 2 hours at room temperature. The solvents were removed by using a rotary evaporator (Rotovap). The product was purified by applying preparative HPLC with a gradient elution consisting of methanol (MeOH) and H_2O. Purity was   95%, and the rude yield was 74%. ^{1}HNMR (MeOH-d_6, 600 MHz): δ 8.95 (1H, s), 8.43 (1H, d, J = 9.5 Hz), 8.02 (1H, d, J = 9.5 Hz), 7.68 (1H, s), 5.61 (1H, d, J = 16.2 Hz), 5.43 (1H, d, J = 16.2 Hz), 5.39 (2H, s), 5.20 (2H, d, J = 2.1 Hz), 4.18 (2H, s), 3.31 (1H, s), 3.03 (6H, s), 1.99 (2H, m), 1.04 (3H, t, J = 7.3 Hz). Calculated values for $C_{26}H_{26}N_3O_5$, $[M+H]^+$, and $C_{52}H_{51}N_6O_{10}$, $[2M+H]^+$, were 460.1871 and 919.3667, respectively; 460.2103 and 919.3643 were found in HRMS (59). All chemical reagents and solvents were commercially purchased from Sigma-Aldrich.

Chem-ChIP

A549 cells (10^8 cells per condition) were pretreated for 1 hour with 100 nM TPT-A or DMSO, infected with influenza PR8 NS1 virus, and, at 1 hour after infection, treated again with TPT-A or DMSO. Cells were collected 6 hours after infection and treated as described above for the ChIP procedure. Sonicated DNA fragments for each condition were separated into 500-μl aliquots. The following reagents were added sequentially with vortexing after each addition: 11.3 μl of 5 mM biotin-azide (final concentration: 100 μM), 11.3 μl of 50 mM tris(2-carboxyethyl) phosphine (TCEP, final concentration: 1 mM), 34 μl of 1.7 mM tris(benzyltriazolylmethyl) amine (TBTA, final concentration: 100 μM), and 11.3 μl of 50 mM copper(II) sulfate pentahydrate ($CuSO_4 \cdot 5H_2O$, final concentration: 1 mM). These mixtures were then incubated at room temperature for 1 hour, with vortexing after the first 30 min. Chromatin aliquots were combined and centrifuged for 5 min at 6500g at 4°C. The supernatant was then removed for downstream immunoprecipitation. ChIP qPCR was performed as described above. The statistical significance of ChIP qPCR analysis was determined with a two-tailed Student's paired t test.

Stranded RNA sequencing and data analysis

RNA (1 μg) was treated using the Ribo-Zero Gold rRNA Removal Kit (Human/Mouse/Rat, Illumina), and purified post-depletion with 1.6× ratio of AMPureXP beads. Directional RNA libraries were prepared using NEBNext Ultra Directional RNA library prep kit for Illumina (New England BioLabs), according to manufacturer's instructions. Fragment size distribution and concentration of the PCR-amplified libraries were assessed using the Qubit and the Agilent Bioanalyzer. Finally, samples were sequenced on the HiSEq 2500 platform in a 100-bp single-end read format.

After adapter removal with cutadapt and base quality trimming to remove 3′ ends if more than 20 bases with Q < 20 were present, reads were mapped to the human (hg19) and Ebola virus (H.sapiens-tc/COD/1976/Yambuku-Mayinga, NC_002549) reference genomes using

STAR (60), and gene and transcript count summaries were generated using Featurecounts (61). Read counts were then combined into a numeric matrix, with genes in rows and experiments in columns, and used as input for differential gene expression analysis with the Bioconductor edgeR package (62). Normalization factors were computed using the weighted trimmed mean of M-values (TMM), and dispersions (common, trended, and tagwise) were estimated before fitting a negative binomial general linearized model that accounted for experimental conditions with two biological replicates each. Finally, a likelihood ratio test was carried against selected contrasts. P values were corrected for multiple testing using the Benjamin-Hochberg (BH) method and used to select genes with significant expression differences ($q < 0.05$).

Proteomic analysis

A549 cells were treated with CPT or DMSO and infected with the influenza PR8 NS1 virus as described above, collected 6 hours after infection, washed three times with PBS [including protease inhibitors (Roche)], then frozen as cell pellets. These pellets were sent to Bioproximity LLC, where global proteomic profiling was acquired using ultraperformance liquid chromatography and tandem mass spectrometry.

For the analysis of mass spectrometry "hits," initial thresholds were calculated in duplicate experiments for protein abundances in both DMSO- and CPT-treated uninfected cells. Next, protein abundances were calculated in the respective infected conditions and normalized using noninfected abundances. We considered up-regulated hits as having a normalized unique protein score above 5 in the DMSO-treated, infected cells. The statistical comparison between normalized infected identifications was determined with a two-tailed Student's t test under the assumption of equal variances between groups.

Transcription factor promoter enrichment analysis

Identification of transcription factors (TFs) regulating the genes affected by Top1 depletion was performed using a computational method that overlaps the genomic coordinates of a set of gene promoters with a large library of TF-genome interactions. We created the ChIP-seq library by compiling 1630 human ChIP-seq data sets from a variety of sources, including ENCODE (63), Cistrome (64), PAZAR (65), and Re-Map (66). As input, we took a set of genomic regions of interest (e.g., promoters of genes whose expression changes upon silencing of Top1) that we systematically overlapped with each ChIP-seq data set, and we counted the number of input regions overlapped by at least one base.

Next, a P value describing the significance of this overlap was estimated using a simulation-based procedure: A distribution of expected overlap values was created from 1000 iterations of randomly choosing RefSeq gene promoters with the same length as the input set (as an example, for 50 promoters of length 100 bp as input, 50 randomly chosen promoters of length 100 bp were used in each simulation). The distribution of the expected overlap values from the randomized data resembled a normal distribution and was used to generate a Z-score and P value estimating the significance of the observed number of input regions that overlapped each ChIP-seq data set. We obtained a ranked list of TFs, based on experimentally-determined binding sites located in the promoters of each gene set. We

applied this procedure to each input gene list using three different promoter definitions, (−100, +1), (−1000, +1), and (−10,000, +1), relative to the transcription start site. Results were similar regardless of promoter length (table S3). We further annotated the results with TF binding site motif enrichment scores (using the same promoter definitions). For this, we used the HOMER motif enrichment algorithm (67) and a large library of human position weight matrices obtained from the CisBP database (68).

Mapping

ChIP-seq data from this study and publicly available data from ENCODE for DNase-seq (GSE26328) and histone H3 Lys^{27} acetylation (H3K27ac; GSE29611) in A549 cells were aligned to the human genome (hg19/GRCh37) using Bowtie2 with default parameters (69). Only reads that mapped to unique genomic positions were considered for downstream analysis. Normalized promoter ChIP-seq read densities were calculated using HOMER (http://homer.salk.edu) by counting the total number of reads per 10^7 aligned reads from each experiment found from −500 to +500 bp relative to the representative RefSeq defined transcription start site (TSS) for each gene (67). META gene plots were compiled by calculating ChIP-seq read densities along RefSeq gene bodies (>3 kb in length) using HOMER. CpG Island promoters were defined by RefSeq TSS found within 200 bp of an annotated CpG Island (70). IFN-stimulated response elements (ISREs) containing promoters were defined by searching for ISRE motifs from −500 to +100 relative to the TSS using HOMER.

Supplementary Material

Refer to Web version on PubMed Central for supplementary material.

ACKNOWLEDGMENTS

REFERENCES AND NOTES

1. Janeway CA Jr. Medzhitov R. Innate immune recognition. Annu. Rev. Immunol. 2002; 20:197–216. doi: 10.1146/annurev.immunol.20.083001.084359; pmid: 11861602. [PubMed: 11861602]

2. Medzhitov R. Approaching the asymptote: 20 years later. Immunity. 2009; 30:766–775. doi: 10.1016/j.immuni.2009.06.004; pmid: 19538928. [PubMed: 19538928]

3. Beutler B, et al. Genetic analysis of resistance to viral infection. Nat. Rev. Immunol. 2007; 7:753–766. doi: 10.1038/nri2174; pmid: 17893693. [PubMed: 17893693]

4. Schoggins JW, et al. A diverse range of gene products are effectors of the type I interferon antiviral response. Nature. 2011; 472:481–485. doi: 10.1038/nature09907; pmid: 21478870. [PubMed: 21478870]

5. Crow YJ. Type I interferonopathies: Mendelian type I interferon up-regulation. Curr. Opin. Immunol. 2015; 32:7–12. doi: 10.1016/j.coi.2014.10.005; pmid: 25463593. [PubMed: 25463593]

6. Hanada T, Yoshimura A. Regulation of cytokine signaling and inflammation. Cytokine Growth Factor Rev. 2002; 13:413–421. doi: 10.1016/S1359-6101(02)00026-6; pmid: 12220554. [PubMed: 12220554]

7. McNab F, Mayer-Barber K, Sher A, Wack A, O'Garra A. Type I interferons in infectious disease. Nat. Rev. Immunol. 2015; 15:87–103. doi: 10.1038/nri3787; pmid: 25614319. [PubMed: 25614319]

8. Brandes M, Klauschen F, Kuchen S, Germain RN. A systems analysis identifies a feedforward inflammatory circuit leading to lethal influenza infection. Cell. 2013; 154:197–212. doi: 10.1016/j.cell.2013.06.013; pmid: 23827683. [PubMed: 23827683]

9. Loo YM, Gale M Jr. Influenza: Fatal immunity and the 1918 virus. Nature. 2007; 445:267–268. doi: 10.1038/445267a; pmid: 17230179. [PubMed: 17230179]

10. Ward PA. New approaches to the study of sepsis. EMBO Mol. Med. 2012; 4:1234–1243. doi: 10.1002/emmm.201201375; pmid: 23208733. [PubMed: 23208733]

11. Strähle L, Garcin D, Le Mercier P, Schlaak JF, Kolakofsky D. Sendai virus targets inflammatory responses, as well as the interferon-induced antiviral state, in a multifaceted manner. J. Virol. 2003; 77:7903–7913. doi: 10.1128/JVI.77.14.7903-7913.2003; pmid: 12829830. [PubMed: 12829830]

12. Beretta GL, Gatti L, Perego P, Zaffaroni N. Camptothecin resistance in cancer: Insights into the molecular mechanisms of a DNA-damaging drug. Curr. Med. Chem. 2013; 20:1541–1565. doi: 10.2174/0929867311320120006; pmid: 23432590. [PubMed: 23432590]

13. Chen Y, et al. Cordycepin induces apoptosis of C6 glioma cells through the adenosine 2A receptor-p53-caspase-7-PARP pathway. Chem. Biol. Interact. 2014; 216:17–25. doi: 10.1016/j.cbi.2014.03.010; pmid: 24704558. [PubMed: 24704558]

14. Kubicek S, et al. Reversal of H3K9me2 by a small-molecule inhibitor for the G9a histone methyltransferase. Mol. Cell. 2007; 25:473–481. doi: 10.1016/j.molcel.2007.01.017; pmid: 17289593. [PubMed: 17289593]

15. Kubo I, Ha TJ, Shimizu K. Lipoxygenase inhibitory activity of 6-pentadecanylsalicylic acid without prooxidant effect. Nat. Prod. Commun. 2010; 5:85–90. pmid: 20184028. [PubMed: 20184028]

16. Menazza S, et al. Oxidative stress by monoamine oxidases is causally involved in myofiber damage in muscular dystrophy. Hum. Mol. Genet. 2010; 19:4207–4215. doi: 10.1093/hmg/ddq339; pmid: 20716577. [PubMed: 20716577]

17. Rahl PB, et al. c-Myc regulates transcriptional pause release. Cell. 2010; 141:432–445. doi: 10.1016/j.cell.2010.03.030; pmid: 20434984. [PubMed: 20434984]

18. Regal KM, Mercer SL, Deweese JE. HU-331 is a catalytic inhibitor of topoisomerase IIα. Chem. Res. Toxicol. 2014; 27:2044–2051. doi: 10.1021/tx500245m; pmid: 25409338. [PubMed: 25409338]

19. Smith NA, Byl JA, Mercer SL, Deweese JE, Osheroff N. Etoposide quinone is a covalent poison of human topoisomerase IIβ. Biochemistry. 2014; 53:3229–3236. doi: 10.1021/bi500421q; pmid: 24766193. [PubMed: 24766193]

20. Zhou Q, Li T, Price DH. RNA polymerase II elongation control. Annu. Rev. Biochem. 2012; 81:119–143. doi: 10.1146/annurev-biochem-052610-095910; pmid: 22404626. [PubMed: 22404626]

21. Filippakopoulos P, Knapp S. Targeting bromodomains: Epigenetic readers of lysine acetylation. Nat. Rev. Drug Discov. 2014; 13:337–356. doi: 10.1038/nrd4286; pmid: 24751816. [PubMed: 24751816]

22. Pommier Y. Topoisomerase I inhibitors: Camptothecins and beyond. Nat. Rev. Cancer. 2006; 6:789–802. doi: 10.1038/nrc1977; pmid: 16990856. [PubMed: 16990856]

23. Nicodeme E, et al. Suppression of inflammation by a synthetic histone mimic. Nature. 2010; 468:1119–1123. doi: 10.1038/nature09589; pmid: 21068722. [PubMed: 21068722]

24. Filippakopoulos P, et al. Selective inhibition of BET bromodomains. Nature. 2010; 468:1067–1073. doi: 10.1038/nature09504; pmid: 20871596. [PubMed: 20871596]

25. Egger G, Liang G, Aparicio A, Jones PA. Epigenetics in human disease and prospects for epigenetic therapy. Nature. 2004; 429:457–463. doi: 10.1038/nature02625; pmid: 15164071. [PubMed: 15164071]

26. Atherton KT, Burke DC. Interferon induction by viruses and polynucleotides: A differential effect of comptothecin. J. Gen. Virol. 1975; 29:297–304. doi: 10.1099/0022-1317-29-3-297; pmid: 1239490. [PubMed: 1239490]

27. Atherton KT, Burke DC. The effects of some differential metabolic inhibitors on interferon superinduction. J. Gen. Virol. 1975; 41:2.

28. Chiou WF, Chou CJ, Chen CF. Camptothecin suppresses nitric oxide biosynthesis in RAW 264.7 macrophages. Life Sci. 2001; 69:625–635. doi: 10.1016/S0024-3205(01)01154-7; pmid: 11476184. [PubMed: 11476184]

29. King IF, et al. Topoisomerases facilitate transcription of long genes linked to autism. Nature. 2013; 501:58–62. doi: 10.1038/nature12504; pmid: 23995680. [PubMed: 23995680]

30. Solier S, et al. Transcription poisoning by Topoisomerase I is controlled by gene length, splice sites, and miR-142-3p. Cancer Res. 2013; 73:4830–4839. doi: 10.1158/0008-5472.CAN-12-3504; pmid: 23786772. [PubMed: 23786772]

31. Kouzine F, et al. Transcription-dependent dynamic supercoiling is a short-range genomic force. Nat. Struct. Mol. Biol. 2013; 20:396–403. doi: 10.1038/nsmb.2517; pmid: 23416947. [PubMed: 23416947]

32. Kretzschmar M, Meisterernst M, Roeder RG. Identification of human DNA topoisomerase I as a cofactor for activator-dependent transcription by RNA polymerase II. Proc. Natl. Acad. Sci. U.S.A. 1993; 90:11508–11512. doi: 10.1073/pnas.90.24.11508; pmid: 8265582. [PubMed: 8265582]

33. Merino A, Madden KR, Lane WS, Champoux JJ, Reinberg D. DNA topoisomerase I is involved in both repression and activation of transcription. Nature. 1993; 365:227–232. doi: 10.1038/365227a0; pmid: 8396729. [PubMed: 8396729]

34. Kohn KW, Pommier Y. Molecular and biological determinants of the cytotoxic actions of camptothecins. Perspective for the development of new topoisomerase I inhibitors. Ann. N.Y. Acad. Sci. 2000; 922:11–26. doi: 10.1111/j.1749-6632.2000.tb07021.x; pmid: 11193886. [PubMed: 11193886]

35. Höing S, et al. Discovery of inhibitors of microglial neurotoxicity acthing thorugh multiple mechanisms using a stem-cell-based phenotypic assay. Cell Stem Cell. 2012; 11:620–632. doi: 10.1016/j.stem.2012.07.005; pmid: 22770236. [PubMed: 23064101]

36. Madabhushi R, et al. Activity-induced DNA breaks govern the expression of neuronal early-reponse genes. Cell. 2015; 161:1592–1605. doi: 10.1016/j.cell.2015.05.032; pmid: 26052046. [PubMed: 26052046]

37. Anders L, et al. Genome-wide localization of small molecules. Nat. Biotechnol. 2014; 32:92–96. doi: 10.1038/nbt.2776; pmid: 24336317. [PubMed: 24336317]

38. Teves SS, Henikoff S. Transcription-generated torsional stress destabilizes nucleosomes. Nat. Struct. Mol. Biol. 2014; 21:88–94. doi: 10.1038/nsmb.2723; pmid: 24317489. [PubMed: 24317489]

39. Ramirez-Carrozzi VR, et al. Selective and antagonistic functions of SWI/SNF and Mi-2β nucleosome remodeling complexes during an inflammatory response. Genes Dev. 2006; 20:282–296. doi: 10.1101/gad.1383206; pmid: 16452502. [PubMed: 16452502]

40. Ramirez-Carrozzi VR, et al. A unifying model for the selective regulation of inducible transcription by CpG islands and nucleosome remodeling. Cell. 2009; 138:114–128. doi: 10.1016/j.cell.2009.04.020; pmid: 19596239. [PubMed: 19596239]

41. Hargreaves DC, Horng T, Medzhitov R. Control of inducible gene expression by signal-dependent transcriptional elongation. Cell. 2009; 138:129–145. doi: 10.1016/j.cell.2009.05.047; pmid: 19596240. [PubMed: 19596240]

42. Smale ST, Natoli G. Transcriptional control of inflammatory responses. Cold Spring Harb. Perspect. Biol. 2014; 6:a016261. doi: 10.1101/cshperspect.a016261; pmid: 25213094. [PubMed: 25213094]

43. Akira S, Uematsu S, Takeuchi O. Pathogen recognition and innate immunity. Cell. 2006; 124:783–801. doi: 10.1016/j.cell.2006.02.015; pmid: 16497588. [PubMed: 16497588]

44. Kim HK, Missiakas D, Schneewind O. Mouse models for infectious diseases caused by *Staphylococcus aureus*. J. Immunol. Methods. 2014; 410:88–99. doi: 10.1016/j.jim.2014.04.007. [PubMed: 24769066]

45. McCullers JA, et al. Influenza enhances susceptibility to natural acquisition of and disease due to *Streptococcus pneumoniae* in ferrets. J. Infect. Dis. 2010; 202:1287–1295. doi: 10.1086/656333; pmid: 20822454. [PubMed: 20822454]

46. Sass G, Koerber K, Bang R, Guehring H, Tiegs G. Inducible nitric oxide synthase is critical for immune-mediated liver injury in mice. J. Clin. Invest. 2001; 107:439–447. doi: 10.1172/JCI10613; pmid: 11181643. [PubMed: 11181643]

47. Bray M, Mahanty S. Ebola hemorrhagic fever and septic shock. J. Infect. Dis. 2003; 188:1613–1617. doi: 10.1086/379727; pmid: 14639530. [PubMed: 14639530]

48. Martínez-Gil L, et al. Identification of small molecules with type I interferon inducing properties by high-throughput screening. PLOS ONE. 2012; 7:e49049. doi: 10.1371/journal. pone.0049049; pmid: 23145065. [PubMed: 23145065]

49. Baum A, Sachidanandam R, García-Sastre A. Preference of RIG-I for short viral RNA molecules in infected cells revealed by next-generation sequencing. Proc. Natl. Acad. Sci. U.S.A. 2010; 107:16303–16308. doi: 10.1073/pnas.1005077107; pmid: 20805493. [PubMed: 20805493]

50. Martínez-Sobrido L, et al. Hemagglutinin-pseudotyped green fluorescent protein-expressing influenza viruses for the detection of influenza virus neutralizing antibodies. J. Virol. 2010; 84:2157–2163. doi: 10.1128/JVI.01433-09; pmid: 19939917. [PubMed: 19939917]

51. Martínez-Gil L, et al. A Sendai virus-derived RNA agonist of RIG-I as a virus vaccine adjuvant. J. Virol. 2013; 87:1290–1300. doi: 10.1128/JVI.02338-12; pmid: 23175362. [PubMed: 23175362]

52. Basler CF, et al. The Ebola virus VP35 protein functions as a type I IFN antagonist. Proc. Natl. Acad. Sci. U.S.A. 2000; 97:12289–12294. doi: 10.1073/pnas.220398297; pmid: 11027311. [PubMed: 11027311]

53. Huang W, Sherman BT, Lempicki RA. Systematic and integrative analysis of large gene lists using DAVID bioinformatics resources. Nat. Protoc. 2009; 4:44–57. doi: 10.1038/nprot.2008.211; pmid: 19131956. [PubMed: 19131956]

54. Huang W, Sherman BT, Lempicki RA. Bioinformatics enrichment tools: Paths toward the comprehensive functional analysis of large gene lists. Nucleic Acids Res. 2009; 37:1–13. doi: 10.1093/nar/gkn923; pmid: 19033363. [PubMed: 19033363]

55. Lee TI, Johnstone SE, Young RA. Chromatin immunoprecipitation and microarray-based analysis of protein location. Nat. Protoc. 2006; 1:729–748. doi: 10.1038/nprot.2006.98; pmid: 17406303. [PubMed: 17406303]

56. Miller MS, et al. Senataxin suppresses the antiviral transcriptional response and controls viral biogenesis. Nat. Immunol. 2015; 16:485–494. doi: 10.1038/ni.3132; pmid: 25822250. [PubMed: 25822250]

57. Swamy KC, Kumar NN, Balaraman E, Kumar KV. Mitsunobu and related reactions: Advances and applications. Chem. Rev. 2009; 109:2551–2651. doi: 10.1021/cr800278z; pmid: 19382806. [PubMed: 19382806]

58. Staker BL, et al. The mechanism of topoisomerase I poisoning by a camptothecin analog. Proc. Natl. Acad. Sci. U.S.A. 2002; 99:15387–15392. doi: 10.1073/pnas.242259599; pmid: 12426403. [PubMed: 12426403]

59. Hyz K, et al. Topotecan dynamics, tautomerism and reactivity—^{1}H/^{13}C NMR and ESI MS study. Magn. Reson. Chem. 2010; 48:575–584. pmid: 20623719. [PubMed: 20623719]

60. Dobin A, et al. STAR: Ultrafast universal RNA-seq aligner. Bioinformatics. 2013; 29:15–21. doi: 10.1093/bioinformatics/bts635; pmid: 23104886. [PubMed: 23104886]

61. Liao Y, Smyth GK, Shi W. featureCounts: An efficient general purpose program for assigning sequence reads to genomic features. Bioinformatics. 2014; 30:923–930. doi: 10.1093/bioinformatics/btt656; pmid: 24227677. [PubMed: 24227677]

62. Robinson MD, McCarthy DJ, Smyth GK. edgeR: A Bioconductor package for differential expression analysis of digital gene expression data. Bioinformatics. 2010; 26:139–140. doi: 10.1093/bioinformatics/btp616; pmid: 19910308. [PubMed: 19910308]

63. ENCODE Project Consortium, An integrated encyclopedia of DNA elements in the human genome. Nature. 2012; 489:57–74. pmid: 22955616. [PubMed: 22955616]

64. Liu T, et al. Cistrome: An integrative platform for transcriptional regulation studies. Genome Biol. 2011; 12:R83. doi: 10.1186/gb-2011-12-8-r83; pmid: 21859476. [PubMed: 21859476]

65. Portales-Casamar E, et al. The PAZAR database of gene regulatory information coupled to the ORCA toolkit for the study of regulatory sequences. Nucleic Acids Res. 2009; 37:D54–D60. doi: 10.1093/nar/gkn783; pmid: 18971253. [PubMed: 18971253]

66. Griffon A, et al. Integrative analysis of public ChIP-seq experiments reveals a complex multi-cell regulatory landscape. Nucleic Acids Res. 2015; 43:e27. doi: 10.1093/nar/gku1280; pmid: 25477382. [PubMed: 25477382]

67. Heinz S, et al. Simple combinations of lineage-determining transcription factors prime cis-regulatory elements required for macrophage and B cell identities. Mol. Cell. 2010; 38:576–589. doi: 10.1016/j.molcel.2010.05.004; pmid: 20513432. [PubMed: 20513432]

68. Weirauch MT, et al. Determination and inference of eukaryotic transcription factor sequence specificity. Cell. 2014; 158:1431–1443. doi: 10.1016/j.cell.2014.08.009; pmid: 25215497. [PubMed: 25215497]

69. Langmead B, Salzberg SL. Fast gapped-read alignment with Bowtie 2. Nat. Methods. 2012; 9:357–359. doi: 10.1038/nmeth.1923; pmid: 22388286. [PubMed: 22388286]

70. Gardiner-Garden M, Frommer M. CpG islands in vertebrate genomes. J. Mol. Biol. 1987; 196:261–282. doi: 10.1016/0022-2836(87)90689-9; pmid: 3656447. [PubMed: 3656447]
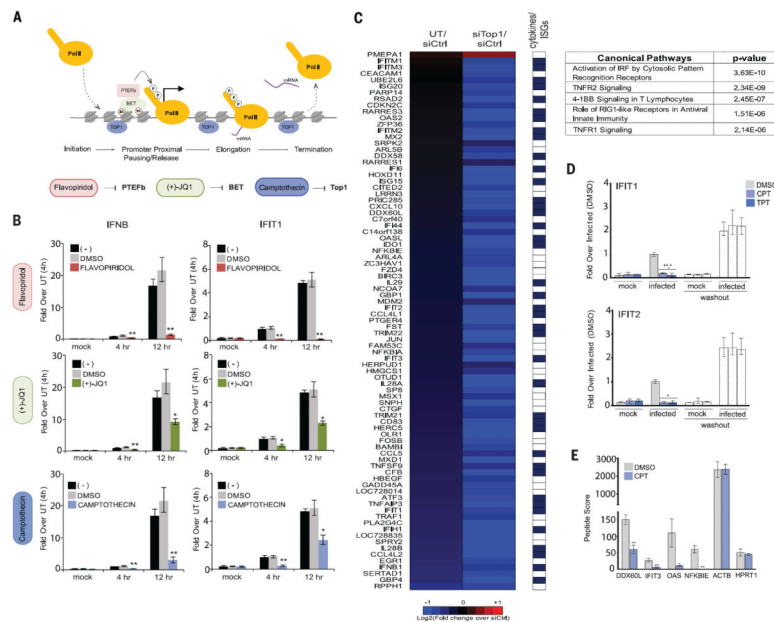
Fig. 1. Top1 inhibition suppresses PAMP-induced gene expression

(**A**) Schematic representation of factors controlling different phases of RNAPII-mediated transcription. Chemical inhibitors FVD (red), (+)-JQ1 (green), and CPT (blue) are color-coded according to their protein targets. (**B**) Quantitative PCR (qPCR) results showing the expression levels of representative viral PAMP-induced genes IFNB and IFIT1, in response to the influenza PR8 ΔNS1 virus infection in A549 cells, either untreated (−) or treated with DMSO or 5 μM inhibitors. (**C**) Heat map showing relative change in gene expression levels in A549 cells not transfected (UT) or transfected with a Top1-specific siRNA (siTop1), as compared to non-targeting control siRNA-treated (siCtrl) cells during infection with influenza PR8 ΔNS1 for genes differentially expressed between siTop1 and siCtrl at 4 hours after infection ($P < 0.01$; ANOVA with post hocTukey HSD test). Known interferon-stimulated genes (ISGs) and cytokine-coding genes are indicated in the adjacent heat map. A table summarizing the top five pathways affected by Top1 depletion during infection is also shown (top right). (**D**) Expression levels of IFIT1 and IFIT2 genes in response to influenza PR8 ΔNS1 infection in A549 cells treated with 0.5 μM CPT, 100 nM TPT, or DMSO at 4 hours after infection (left bars) or 16 hours after washout (white, right bars). (**E**) Mass spectrometry data showing representative virus-induced and housekeeping protein levels in response to influenza PR8 ΔNS1 infection in A549 cells treated with 0.5 μM CPTor DMSO at 6 hours after infection. *$P < 0.05$, **$P < 0.005$ (Student's *t* test with Holm-Bonferroni sequential correction). Data are means ± SD from three [(B) to (D)] and two (E) independent experiments.
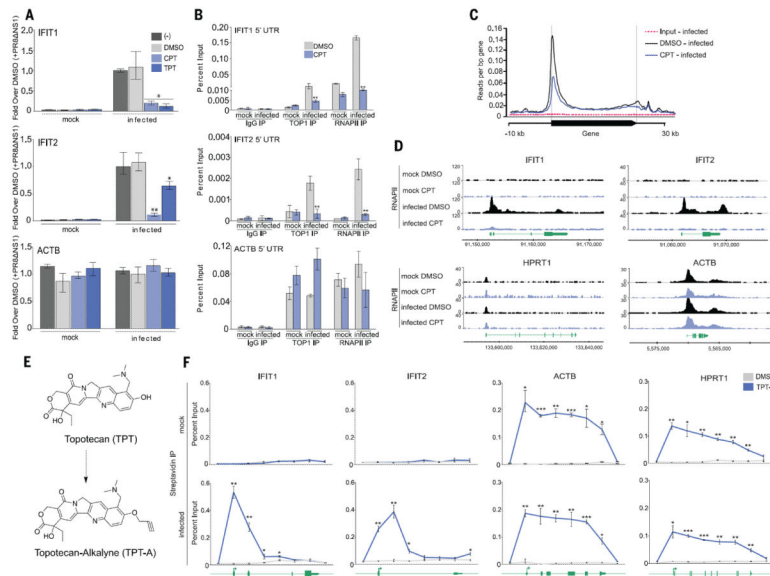
Fig. 2. Topotecan (TPT) and camptothecin (CPT) suppress RNAPII at PAMP-induced genes
(**A**) Gene expression in human A549 cells, left untreated (−) or treated with 0.5 μM CPT, 100 nM TPT, or DMSO, at 4 hours after mock treatment or PR8 NS1 virus infection. (**B**) ChIP-qPCR analysis of endogenous RNAPII and Top1 at the promoters of IFIT1, IFIT2, and ACTB in A549 cells treated with 0.5 μM CPT or DMSO, at 4 hours after mock treatment or infection with influenza PR8 NS1. (**C**) ChIP-seq metaplot of endogenous RNAPII in A549 cells treated with 0.5 μM CPT or DMSO 6 hours after mock treatment or PR8 NS1 virus infection. Plots represent RNAPII occupancy at genes showing a factor of 2 up-regulation in their expression after infection. (**D**) ChIP-seq tracks of representative antiviral genes IFIT1 and IFIT2, and housekeeping genes ACTB and HPRT1. (**E**) Schematic representation of the chemical synthesis of TPT-A from TPT. (**F**) Chem-ChIP qPCR analysis of TPT-A occupancy across IFIT1, IFIT2, ACTB, and HPRT1 genes in A549 cells treated with DMSO or 100 nM TPT-A, at 6 hours after mock treatment or PR8 NS1 infection. $*P < 0.05$, $**P < 0.005$, $***P < 0.0005$ (Student's t test with Holm-Bonferroni sequential correction). Data are means ± SD from three (A) and two [(B) and (F)] independent experiments.
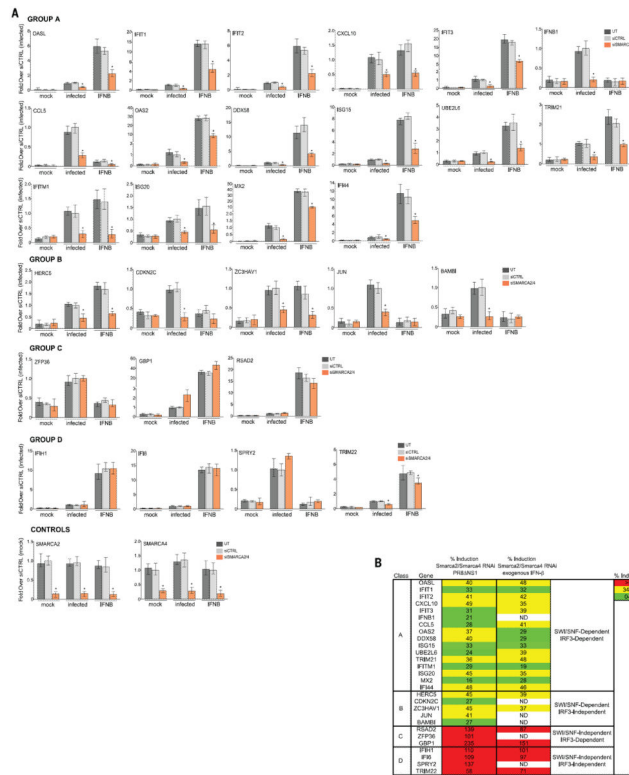
Fig. 3. Classification of SMARCA2/4-dependent PAMP-induced genes

(**A**) Expression of genes up-regulated by a factor of >2 after infection and suppressed by Top1 inhibition in A549 cells at 4 hours after mock treatment, infection with PR8 ΔNS1 virus (infected), or stimulation with exogenous IFN-β (IFNB). Cells were dual-transfected with siRNAs targeting SMARCA2 and SMARCA4 (orange bars). SWI/SNF dependency was evaluated via transient knockdown of SMARCA2/4, and IRF3-dependent genes were compiled from the literature and cross-compared with a list of genes induced by IRF35D in STAT1$^{-/-}$ cells. (**B**) Table summarizing the results for genes in (A). Columns 2 and 3 show the effect of SMARCA2/4 knockdown on PR8 ΔNS1 and exogenous interferon (IFN-β)–induced mRNA levels, respectively. Levels of mRNA are shown as a percentage of the mRNA level determined by qPCR in siCtrl-treated A549 cells (set at 100% for each gene). Column 4 classifies the genes: A and B (21/28 genes) are SWI/SNF-dependent (inducibility levels <50%), C and D (7/28) are SWI/SNF-independent (inducibility >50%). Color-coded legends for columns 2 and 3 are shown at the top right. *$P < 0.05$ (Student's t test with Holm-Bonferroni sequential correction). Data are means ± SD from three independent experiments.
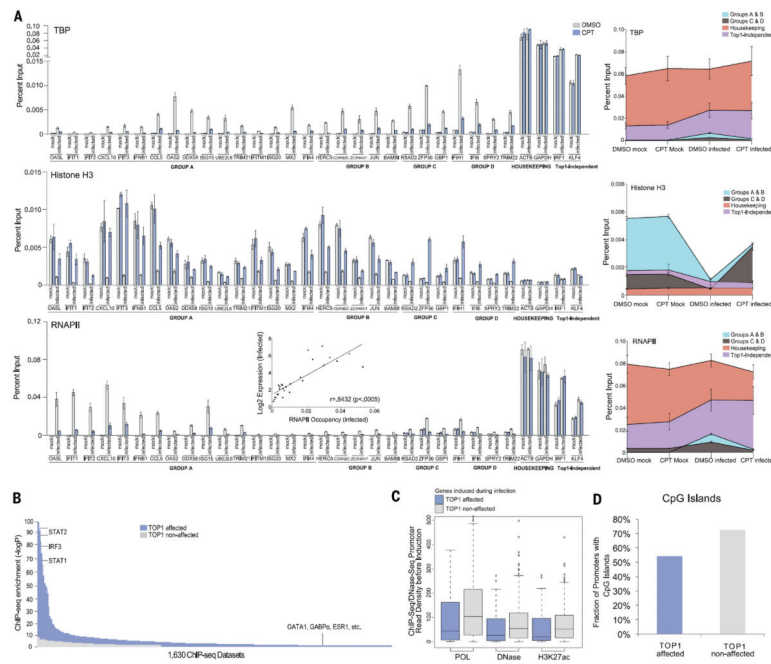
Fig. 4. Top1 inhibition suppresses PAMP-induced genes that require nucleosome remodeling for activation

(**A**) Left: ChIP-qPCR analysis of endogenous TBP, histone H3, and RNAPII at the promoters of classes A to D, housekeeping, and PAMP-induced Top1-independent genes (IRF1, KLF4) in A549 cells treated with 0.5 μM CPT or DMSO, at 6 hours after mock treatment or infection with influenza PR8 NS1. Right: Summation plots of each individual protein's occupancy (percent input). Inset: Correlation plot of gene expression (infected) versus RNAPII occupancy (infected) for genes shown in Fig. 3A. Data are means ± SD from two independent experiments. (**B**) Results of testing of 1630 ChIP-seq data sets for transcription factor (TF) enrichment at the promoters of Top1-affected genes during infection (see materials and methods). Negative log of the *P* value of each of these data sets (blue) and results of the same procedure are applied to genes unaffected by Top1 depletion (gray). The displayed data are the result of defining promoters as (−1000, +1) relative to the transcriptional start site. The top three TFs and examples of insignificant TFs are shown. (**C**) Basal state meta-analysis of RNAPII (POL) occupancy, DNase hypersensitivity, and H3K27ac occupancy at the promoters of genes designated as either Top1 affected (*N* = 84) or Top1 nonaffected (*N* = 296) after infection. Data sets used are from ENCODE (see materials and methods). (**D**) Basal state meta-analysis of CpG island occupancy at the promoters of genes designated as either Top1 affected or Top1 nonaffected after infection.
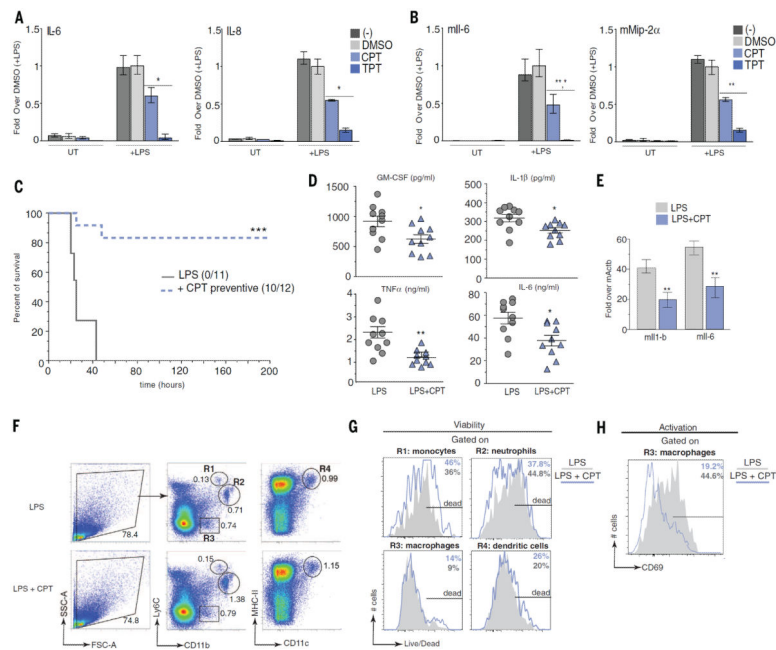
Fig. 5. Top1 regulates LPS-induced inflammation in vitro and in vivo
(**A** and **B**) Gene expression in A549 (A) or RAW 264.7 (B) cells, left untreated (−) or treated with 0.5 μM CPT, 100 nM TPT or DMSO, in the presence of LPS stimulation or not (UT). (**C** to **H**) C57BL/6J mice left untreated or treated with CPT in response to LPS-induced septic shock. (C) Survival curve. (D) Serum titers of indicated cytokines at 4 hours after LPS injection. [(E) to (H)] Ninety minutes after LPS injection spleens were harvested to perform transcriptional analysis of indicated inflammatory genes (E) and to determine cell viability and activation by flow cytometry [(F) to (H)]. (F) Gating strategy. (G) Histograms comparing the incorporation of a live/dead dye after gating on R1, R2, R3, and R4. (H) CD69 expression after gating on R3. $*P < 0.05$, $**P < 0.005$, $***P < 0.0005$ (Student's t test with Holm-Bonferroni sequential correction) for [(A), (B), (D), (E)] or log rank test (C). Data are means ± SD from three independent experiments [(A) to (C)] with $n = 11$ (LPS) and $n = 12$ (LPS + CPT) individual mice, or two independent experiments [(D) to (H)] with $n = 6$ (LPS) and $n = 7$ CPT (LPS + CPT) individual mice.
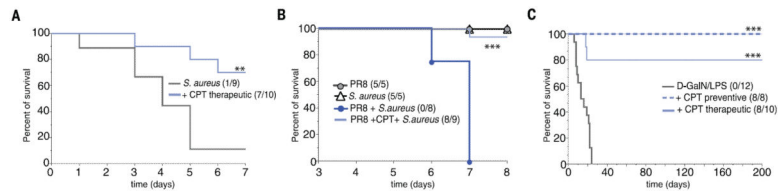
Fig. 6. Top1 inhibition blocks lethal inflammation in vivo

(**A** to **C**) Survival curves of C57BL/6J mice left untreated or treated with CPT in response to *S. aureus* infection (A), PR8–*S. aureus* co-infection (B), or D-GalN/LPS injection (C). Mice were treated with CPT 3, 24, and 48 hours after *S. aureus* infection (A); 12, 24, and 36 hours after PR8 infection (B); or 2 hours and 30 min after D-GalN/LPS injection (C). **P < 0.005, ***P < 0.0005 (log rank test). Data are from three independent experiments (A) with *n* = 8 to 12 individual mice, and two independent experiments [(B) and (C)] with *n* = 5 to 9 individual mice.
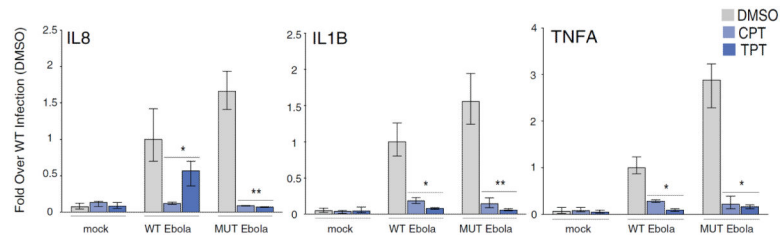
Fig. 7. Suppression of Ebola virus induced inflammation by Top1 inhibitors

THP-1 cells were mock-treated or infected with wild-type (WT) Ebola virus (Zaire-Mayinga strain) in the presence of 0.5 μM CPT, 100 nM TPT, or DMSO. Bar graphs show the relative expression of selected genes. Data are means ± SD from three independent experiments. $*P < 0.05$, $**P < 0.005$ (Student's t test with Holm-Bonferroni sequential correction).